



Calhoun: The NPS Institutional Archive

Theses and Dissertations

Thesis Collection

2007-12

Design and performance evaluation study of a
prototype of a tactical unmanned aerial vehicle

Teng, Choon Hon Adrian

Monterey, California. Naval Postgraduate School

<http://hdl.handle.net/10945/3043>



Calhoun is a project of the Dudley Knox Library at NPS, furthering the precepts and goals of open government and government transparency. All information contained herein has been approved for release by the NPS Public Affairs Officer.

Dudley Knox Library / Naval Postgraduate School
411 Dyer Road / 1 University Circle
Monterey, California USA 93943

<http://www.nps.edu/library>



**NAVAL
POSTGRADUATE
SCHOOL**

MONTEREY, CALIFORNIA

THESIS

**DESIGN AND PERFORMANCE EVALUATION STUDY OF
A PROTOTYPE OF A TACTICAL UNMANNED AERIAL
VEHICLE**

by

Teng Choon Hon Adrian

December 2007

Thesis Advisors:

Kevin D. Jones

Vladimir N. Dobrokhodov

Approved for public release; distribution is unlimited

THIS PAGE INTENTIONALLY LEFT BLANK

REPORT DOCUMENTATION PAGE			<i>Form Approved OMB No. 0704-0188</i>
Public reporting burden for this collection of information is estimated to average 1 hour per response, including the time for reviewing instruction, searching existing data sources, gathering and maintaining the data needed, and completing and reviewing the collection of information. Send comments regarding this burden estimate or any other aspect of this collection of information, including suggestions for reducing this burden, to Washington headquarters Services, Directorate for Information Operations and Reports, 1215 Jefferson Davis Highway, Suite 1204, Arlington, VA 22202-4302, and to the Office of Management and Budget, Paperwork Reduction Project (0704-0188) Washington DC 20503.			
1. AGENCY USE ONLY (Leave blank)	2. REPORT DATE December 2007	3. REPORT TYPE AND DATES COVERED Master's Thesis	
4. TITLE AND SUBTITLE Design and Performance Evaluation Study of a Prototype of a Tactical Unmanned Aerial Vehicle		5. FUNDING NUMBERS	
6. AUTHOR(S) Teng Choon Hon Adrian		8. PERFORMING ORGANIZATION REPORT NUMBER	
7. PERFORMING ORGANIZATION NAME(S) AND ADDRESS(ES) Naval Postgraduate School Monterey, CA 93943-5000		10. SPONSORING/MONITORING AGENCY REPORT NUMBER	
9. SPONSORING /MONITORING AGENCY NAME(S) AND ADDRESS(ES) N/A		11. SUPPLEMENTARY NOTES The views expressed in this thesis are those of the author and do not reflect the official policy or position of the Department of Defense or the U.S. Government.	
12a. DISTRIBUTION / AVAILABILITY STATEMENT Approved for public release; distribution is unlimited		12b. DISTRIBUTION CODE	
13. ABSTRACT (maximum 200 words) This thesis aims to provide a low-cost solution through integrating commercial off-the-shelf (COTS) technologies to produce a prototype of a "Tactical Unmanned Combat Aerial Vehicle UCAV" system that can be utilized by the front-line ground units in the near future. The Tactical UCAV is designed to enhance the information collection and autonomous precision strike capability of the ground units. The Tactical UCAV can also be deployed as sensor nodes as part of a larger global information grid in a network-centric warfare operation. The proposed Tactical UCAV system is comprised of a Hunter Unmanned Aerial Vehicle (HUAV), which primarily carries high resolution sensors and communication devices and is used as a mother-ship for smaller "Killer UAVs (KUAV)." The KUAV carries a mission specific set of instruments; it can be a sensor or a warhead or both depending on the desired end results. After the target is acquired by the HUAV, the target information will be transferred to the KUAV. The KUAV can then be launched in close proximity of the target with the target position update from the HUAV. This thesis will focus on the development of a prototype KUAV and the integration of the prototype with the existing HUAV "Rascal" developed and operated by the Naval Postgraduate School (NPS). The KUAV and the HUAV will form the Tactical UCAV system.			
14. SUBJECT TERMS Unmanned Aerial Vehicle, UAV, Tactical UCAV, Non-Powered Glider, Commercial off-the-shelf, Simulink, <i>LinAir</i> , Hardware-in-the-loop, Procerus, Kestrel Autopilot, Kestrel Virtual Cockpit, Aviones		15. NUMBER OF PAGES 117	16. PRICE CODE
17. SECURITY CLASSIFICATION OF REPORT Unclassified	18. SECURITY CLASSIFICATION OF THIS PAGE Unclassified	19. SECURITY CLASSIFICATION OF ABSTRACT Unclassified	20. LIMITATION OF ABSTRACT UU

NSN 7540-01-280-5500

Standard Form 298 (Rev. 2-89)
Prescribed by ANSI Std. Z39-18

THIS PAGE INTENTIONALLY LEFT BLANK

Approved for public release; distribution is unlimited

**DESIGN AND PERFORMANCE EVALUATION STUDY OF A PROTOTYPE OF
A TACTICAL UNMANNED AERIAL VEHICLE**

Teng Choon Hon Adrian
Captain, Singapore Armed Forces (Army)
B.Eng (M.E.), Nanyang Technological University, 2002

Submitted in partial fulfillment of the
requirements for the degree of

MASTER OF SCIENCE IN MECHANICAL ENGINEERING

from the

**NAVAL POSTGRADUATE SCHOOL
December 2007**

Authors: Teng Choon Hon Adrian

Approved by: Kevin D. Jones, PhD
Thesis Advisor

Vladimir N. Dobrokhodov, PhD
Thesis Advisor

Anthony J. Healey, PhD
Chairman, Department of Mechanical and Astronautical
Engineering (MAE)

THIS PAGE INTENTIONALLY LEFT BLANK

ABSTRACT

The Unmanned Aerial Vehicle (UAV) plays a critical role in the current battlefield in the areas of information superiority, collateral damage, urban area fighting and precision strike against high payoff targets. The desire for a shorter “kill-chain” is driving the evolution of the Unmanned Combat Aerial Vehicle (UCAV). However, due to high cost and limited quantities, UCAVs are currently only available to military planners at the operational or strategic level.

This thesis aims to provide a low-cost solution through integrating commercial off-the-shelf (COTS) technologies to produce a prototype of a “Tactical Unmanned Combat Aerial Vehicle UCAV” system that can be utilized by the front-line ground units in the near future. The Tactical UCAV is designed to enhance the information collection and autonomous precision strike capability of the ground units. The Tactical UCAV can also be deployed as sensor nodes as part of a larger global information grid in a network-centric warfare operation.

The proposed Tactical UCAV system is comprised of a Hunter Unmanned Aerial Vehicle (HUAV), which primarily carries high resolution sensors and communication devices and is used as a mother-ship for smaller “Killer UAVs (KUAV).” The KUAV carries a mission specific set of instruments; it can be a sensor or a warhead or both depending on the desired end results. After the target is acquired by the HUAV, the target information will be transferred to the KUAV. The KUAV can then be launched in close proximity of the target with the target position update from the HUAV.

This thesis will focus on the development of a prototype KUAV and the integration of the prototype with the existing HUAV “Rascal” developed and operated by the Naval Postgraduate School (NPS). The KUAV and the HUAV will form the Tactical UCAV system.

THIS PAGE INTENTIONALLY LEFT BLANK

TABLE OF CONTENTS

I.	INTRODUCTION.....	1
A.	OPERATIONAL REQUIREMENTS.....	1
B.	PROPOSED CONCEPT OF OPERATIONS	2
C.	SCOPE AND OBJECTIVES	4
D.	THESIS ORGANIZATION.....	4
II.	LITERATURE REVIEW	7
A.	EXISTING UCAV SYSTEMS.....	7
1.	Predator B – General Atomics Aeronautical Systems, USA.....	7
2.	Sperwer B – Sagem, France	8
B.	EXISTING TACTICAL UAV SYSTEMS.....	8
1.	Shadow 200 – AAI Corporation, USA	9
2.	Watchkeeper Tactical UAV – Thales, UK.....	10
III.	BUILDING THE PROTOTYPE.....	11
A.	PROTOTYPE DESIGN	11
1.	Dimensions.....	12
2.	Material.....	13
3.	Components and Loading	13
4.	Trimming and Balancing	13
5.	Completed Prototype.....	14
IV.	AERODYNAMICS STUDIES.....	17
A.	BASIC AERODYNAMICS FOR GLIDERS	17
B.	SIMULATION USING ANALYTICAL TECHNIQUES	18
1.	Verification of Panel Codes.....	19
2.	Geometry and Input File	20
3.	Aerodynamic Data	21
C.	ANALYTICAL TRADEOFF STUDIES.....	21
1.	Tradeoff Study 1 – L/D vs. AOA	21
2.	Tradeoff Study 2 – γ vs. L/D	23
3.	Tradeoff Study 3 – R vs. L/D	24
4.	Tradeoff Study 4 – V vs. AOA	25
5.	Tradeoff Study 5 – E vs. V	26
V.	GUIDANCE AND CONTROL.....	31
A.	SIMULATION USING NUMERICAL TECHNIQUES.....	31
1.	Analytical Results from <i>LinAir</i>	32
2.	6 Degree of Freedom (DOF) + Auto Pilot (AP) Simulink Model...32	
3.	Modeling the Prototype KUAV in the 6DOF + AP Model.....34	
4.	Simulation Procedures.....	35
5.	Results and Comparisons	36
6.	Refinement of Operational Envelope.....	40

VI.	HARDWARE-IN-THE-LOOP EXPERIMENTS.....	43
A.	ARCHITECTURE AND SETUP	43
1.	Architecture.....	43
2.	Setup.....	45
B.	TUNING AUTOPILOT PID GAINS.....	45
1.	Aerodynamic Performance Parameters	46
2.	Autopilot PID Gains	46
C.	TEST SCENARIOS AND PROCEDURES.....	46
1.	Test Scenarios and Procedures	47
D.	RESULTS AND COMPARISON.....	47
1.	Results	47
2.	Comparison	48
VII.	CONCLUSIONS	53
A.	CONCLUSIONS	53
B.	RECOMMENDATIONS AND FUTURE STUDIES	53
1.	Understanding the Kestrel Autopilot.....	54
2.	Variations to Gliding Profile.....	54
3.	Physical Integration with “Rascal”	54
4.	Data Integration with “Rascal”	54
5.	Variable Payload Capability for the KUAV.....	56
APPENDIX A.	TECHNICAL SPECIFICATIONS OF PREDATOR B.....	57
APPENDIX B.	TECHNICAL SPECIFICATIONS OF SPERWER B	59
APPENDIX C.	TECHNICAL SPECIFICATIONS OF SHADOW 200.....	61
APPENDIX D.	TECHNICAL SPECIFICATIONS OF WATCHKEEPER TACTICAL UAV.....	63
APPENDIX E.	COMPONENT SPECIFICATIONS	65
APPENDIX F.	VERIFICATION OF PANEL CODES.....	67
APPENDIX G.	INPUT FILE FOR PANEL CODE	71
APPENDIX H.	DATA FILE GENERATED BY PANEL CODE.....	73
APPENDIX I.	INITIALIZATION FILE FOR 6DOF + AP MODEL	75
APPENDIX J.	SIMULATION RESULTS FROM THE 6DOF + AP MODEL	77
APPENDIX K.	PROCEDURES FOR SETTING UP THE TCP/IP CONNECTION.....	79
APPENDIX L.	PROCEDURES FOR UPDATING AERODYNAMIC PERFORMANCE PARAMETERS IN AVIONES	85
APPENDIX M.	PID GAINS FOR PROTOTYPE ON KESTREL AUTOPILOT..	87
APPENDIX N.	PROCEDURES FOR RUNNING THE HIL EXPERIMENTS	89
APPENDIX O.	SIMULATION RESULTS FROM HIL	95

LIST OF REFERENCES	97
INITIAL DISTRIBUTION LIST	99

THIS PAGE INTENTIONALLY LEFT BLANK

LIST OF FIGURES

Figure 1.	Proposed concept of operations	3
Figure 2.	Predator B armed with Hellfire missiles	7
Figure 3.	Sperwer B armed with Spike LR missiles	8
Figure 4.	Shadow 200 being launched from a catapult	9
Figure 5.	Watchkeeper Tactical UAV	10
Figure 6.	Plan view of prototype and cross section of EH 3.0/12	12
Figure 7.	Location of aerodynamic center and CG	14
Figure 8.	Components for autonomous flight	14
Figure 9.	Side and top views of the prototype KUAV	15
Figure 10.	Forces acting on a glider in flight	17
Figure 11.	Geometry of glider generated by <i>LinAir</i>	20
Figure 12.	Tradeoff between L/D and AOA	22
Figure 13.	Tradeoff between γ , L/D and AOA	23
Figure 14.	Glide path geometry	24
Figure 15.	Tradeoff between R , L/D and AOA	25
Figure 16.	Tradeoff between V and AOA	26
Figure 17.	Tradeoff between E , V and AOA	27
Figure 18.	Comparison between R and E vs. AOA	28
Figure 19.	Flow chart depicting simulation process	31
Figure 20.	Simulink Block Diagram for 6DOF + AP Model	32
Figure 21.	Comparison between analytical and 6DOF + AP models for L/D vs. AOA	37
Figure 22.	Comparison between analytical and 6DOF + AP models for V vs. AOA	38
Figure 23.	Comparison between analytical and 6DOF + AP models for R vs. AOA	39
Figure 24.	Comparison between analytical and 6DOF + AP models for E vs. AOA	40
Figure 25.	HIL architecture using a TCP/IP connections	44
Figure 26.	HIL architecture using a standard serial modem interface	44
Figure 27.	HIL results for a gliding velocity of 8m/s	48
Figure 28.	Comparison between analytical, 6DOF + AP and HIL models for L/D vs. AOA	49
Figure 29.	Comparison between analytical, 6DOF + AP and HIL models for R vs. AOA	50
Figure 30.	Comparison between analytical, 6DOF + AP and HIL models for E vs. AOA	51
Figure 31.	Communication protocol via ground control stations	55
Figure 32.	Communication protocol via radio frequency module	55
Figure 33.	Disconnected programming wire	79
Figure 34.	Connection for the programming and power cables on autopilot	79
Figure 35.	HIL selection in Virtual Cockpit	80
Figure 36.	Connection window for Aviones	80
Figure 37.	Agent added in Aviones	81
Figure 38.	HIL simulation control window	82
Figure 39.	User interfaces for Aviones and Virtual Cockpit	83

Figure 40.	Aerodynamic performance coefficients for prototype	85
Figure 41.	Physics parameter editor window	86
Figure 42.	Values of PID gains	87
Figure 43.	Flight control window of Virtual Cockpit	89
Figure 44.	Launching the UAV from Aviones.....	90
Figure 45.	UAV in “NAV” mode	91
Figure 46.	HIL Sim Control Window of Aviones.....	92
Figure 47.	Data log window of Virtual Cockpit.....	92

LIST OF TABLES

Table 1.	Dimensions of prototype.....	12
Table 2.	Wind tunnel results of C_{D_0} and K for wings of AR 1 and 2.....	20
Table 3.	Comparison between experimental and analytical results	23

THIS PAGE INTENTIONALLY LEFT BLANK

ACKNOWLEDGMENTS

The completion of this thesis would not be possible without Professor Vladimir Dobrokhodov and Professor Kevin Jones.

I would like to thank Professor Vladimir Dobrokhodov for his support and patience for the entire duration of this thesis. I am grateful for his effort in spending endless hours explaining difficult concepts and Simulink diagrams to me in his office. He has truly shown me what teaching is all about.

I would also like to thank Professor Kevin Jones for all his support and assistance for the entire duration of this thesis. Without his assistance the prototype would never have been built. I will always remember the many hours we spent in the Unmanned System Laboratory cutting the Spyder foam and I will definitely not forget the “pleasant” fumes and particles we had to inhale.

Finally, the advisor and student partnership will come to an end after I graduate from NPS, but I sincerely know that the friendship we built will last for many years to come.

THIS PAGE INTENTIONALLY LEFT BLANK

I. INTRODUCTION

A. OPERATIONAL REQUIREMENTS

Combat missions in the past ten years have proved beyond any doubt that the dependence on the Unmanned Aerial Vehicle (UAV) has increased significantly. The demand for UAVs has evolved from conventional hot-war engagements to low-intensity conflicts such as peacekeeping and humanitarian missions. The demand is so great that it has outpaced the ability for research and development of UAVs to meet the wide spectrum of operational requirements.

The UAVs in the current battlefield play a critical role in areas such as information superiority, collateral damage, urban area fighting and precision strikes against high payoff targets. The three main areas that have been identified for future UAV developments include the growth in size of strategic UAVs for greater payload and endurance, reduction in size of tactical UAVs and the addition of weapons to UAVs to offer lethal capabilities in combat missions [1].

The desire of shorter “kill-chain”—the time from when the target is spotted by a sensor until a shooter locks on—is the main force driving the evolution of the Unmanned Combat Aerial Vehicle (UCAV). The current trend towards asymmetrical warfare, where 90% of the targets are mobile or of the “emerging” variety, emphasizes this even more. The effects of a short “kill-chain” are less apparent at the operational and strategic levels, while the values of rapid targeting are obvious at the tactical level of war. If the process is slow, time critical opportunities may be lost or mobile targets may be long gone by the time an air strike arrives. The faster the attack, the less time the enemy has to react, adjust, adapt, mount a counter-offensive or escape [2].

This thesis aims to provide a low-cost solution through integrating commercial off-the-shelf (COTS) technologies to produce a tactical hunter-killer system that satisfies the needs for both the reduction in size of tactical UAVs and the weaponization of UAVs to offer lethal capability.

B. PROPOSED CONCEPT OF OPERATIONS

The proposed tactical hunter-killer system is better known as Tactical Unmanned Combat Aerial Vehicle or Tactical UCAV. Currently, due to high cost and limited quantities, UCAVs are only made available to military planners at the operational or strategic level. Low-cost production through integrating commercial off-the-shelf technologies will be the driver for making such superior war-fighting capabilities accessible to ground units in the near future.

The Tactical UCAV is designed to enhance the information collection and autonomous precision strike capability of the ground units. The Tactical UCAV can also be deployed as sensor nodes as part of a larger global information grid in a network-centric warfare operation. The proposed concept of operations for the Tactical UCAV is shown in Figure 1 and can be summarized as follows:

A Hunter Unmanned Aerial Vehicle (HUAV) carries high-resolution sensors and communication devices. As the name implies, the HUAV will predominantly play the hunter roll in the proposed Tactical UCAV system. She is configurable to carry one or many of Killer Unmanned Aerial Vehicles (KUAV), and in this aspect she can be thought of as the “Mother Ship” or the air command center for the KUAVs.

The KUAV can be configured to carry a payload of a sensor, a warhead or both, and it will predominantly play the roll of the killer in the proposed system.

After the target is located by the hunter, the information about the target will be “transferred” to the killer. The killer will then be autonomously launched from the mother ship. The killer vehicle will autonomously maneuver to the target with the help of constant updates from the mother ship as to the position of the target.

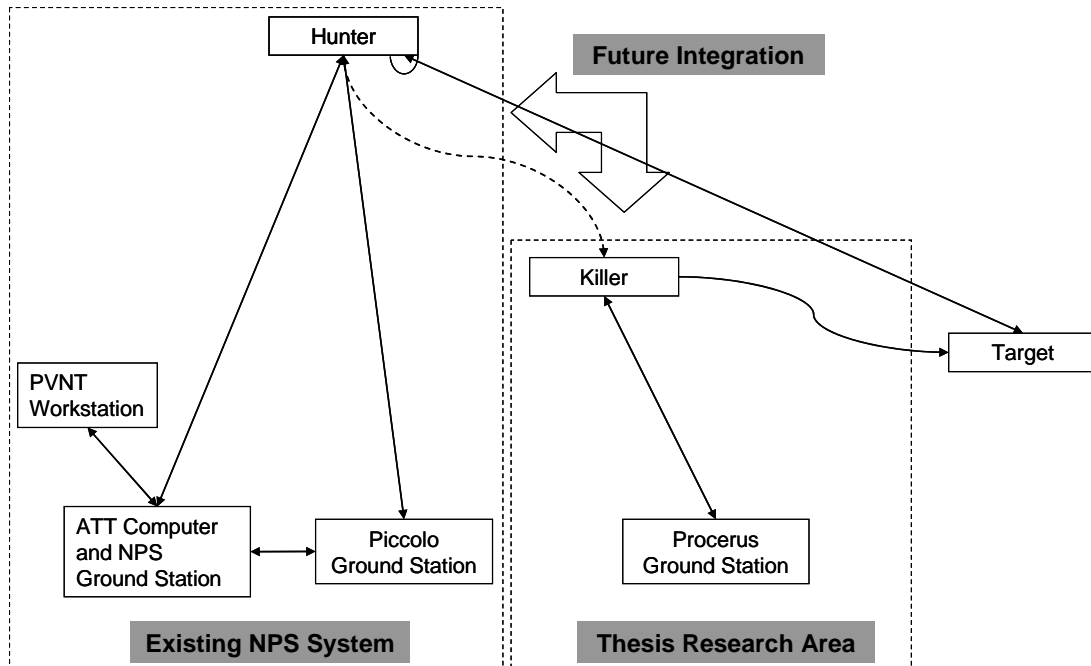


Figure 1. Proposed concept of operations

The Tactical UCAV system is designed to be configurable and low cost, so it can be deployed as a single system or in numbers (swarm) to fulfill many operation requirements. The possibilities include:

Single System

Hunt and Kill Mission. As the name implies, upon acquiring a high-payoff target by the hunter, a killer will be launched to destroy the target.

Continuous Surveillance Mission. Instead of destroying the target, the “killer” carrying surveillance equipment can be launched to close in or follow the target for continuous surveillance.

Multiple Systems (Swarm)

Hunt and Kill Mission. This is similar to the first single system mission. However, it would be used when multiple targets, such as a column of tanks, are to be engaged simultaneously. Multiple Tactical UCAVs can be assembled in the area of operation. If each launches two killer vehicles, a swarm of killers is now available to simultaneously engage the targets.

Continuous Surveillance Mission. A single system has a limited area of coverage in any surveillance mission. A swarm of sensors forming a sensor grid can be deployed to cover a large area or track a moving target with greater tracking accuracy. This operation can also be part of the global information or sensor grids in a network-centric warfare operation.

C. SCOPE AND OBJECTIVES

It can be seen from Figure 1 that this thesis will focus on the development of a prototype KUAV. Due to the limited duration available for this thesis, the integration of the prototype KUAV with the existing HUAV “Rascal” [3] developed and operated by the Naval Postgraduate School (NPS) will be done in the near future. The combination of the prototype KUAV with the existing HUAV will form the Tactical UCAV system.

The scope of this thesis includes the following:

Development of Prototype

Design and build the test prototype

Aerodynamic performance analysis with linear panel software

Tradeoff studies for various performance parameters

Guidance and control analysis with numerical methods

Definition of engagement envelope

Hardware-in-the-Loop Testing

Architecture and setup

Procedures for working with Procerus Virtual Cockpit 2.4.2

Refining engagement envelope

D. THESIS ORGANIZATION

Chapter II provides background on the UCAV and Tactical UAV systems currently in service or development. Chapter III presents the critical considerations and

decisions made for the design and building of the prototype. In Chapter IV, the methodology and tools used for generating aerodynamics performance data from linear panel codes will be discussed. Subsequently, the results of the tradeoff studies for key performance parameters of the prototype will be presented. In Chapter V, the methodology and simulations used for modeling the practical operating environment with numerical techniques will be discussed. The results of the simulations will also be presented in this chapter. In Chapter VI, the setup, procedures, results and findings obtained from Hardware-in-the-Loop (HIL) experiments will be discussed. Finally in Chapter VII, the conclusion and recommendations for future works will be discussed.

THIS PAGE INTENTIONALLY LEFT BLANK

II. LITERATURE REVIEW

A. EXISTING UCAV SYSTEMS

Major UAV systems have been well developed over the years. In recent years, much work and effort have been invested in the development of hybrid systems to reduce the time required in the sensor-to-shooter targeting cycle. These hybrid systems primarily integrate the sensor and shooter in a single platform more commonly known as Unmanned Combat Air Vehicles (UCAV). As part of the literature review, two in-service UCAVs are presented.

1. Predator B – General Atomics Aeronautical Systems, USA

The Predator B aircraft was developed by General Atomics Aeronautical Systems, USA, in 2000 and its flight commencing in February 2001. Powered by a turboprop engine, the Predator B series was designed as a long endurance, high-altitude unmanned aircraft for use as a multi-mission system. From reconnaissance, surveillance, targeting and weapons delivery to scientific research and other civilian applications, Predator B has the capacity to conduct multiple missions simultaneously due to its large internal and external payload capacity. The detailed technical specifications are presented in Appendix A. [4]



Figure 2. Predator B armed with Hellfire missiles

2. Sperwer B – Sagem, France

Sperwer B was designed and developed by Sagem, France, to support Intelligence, Surveillance, Target Acquisition and Reconnaissance (ISTAR) at the battlegroup level. Sperwer is capable of carrying multiple payloads ranging from Forward Looking Infra-Red (FLIR), Electro Optic / Infra-Red (EO/IR) and Synthetic Aperture Radar (SAR). It is equipped with two underwing hardpoints that can carry external loads of up to 30kg each. Sagem has already demonstrated the integration of Sperwer B with the Spike LR missile. They are cooperating with GIAT, to test a new smart munition delivery system, based on the Bonus submunition. However, the armed configuration requires that up to 20 kg of fuel must be removed. This will limit the endurance of the armed Sperwer. The detailed technical specifications are presented in Appendix B. [5]



Figure 3. Sperwer B armed with Spike LR missiles

B. EXISTING TACTICAL UAV SYSTEMS

The development of the Tactical UAV has also progressed significantly in recent years. They are evolving into multi-role, multi-mission platforms. As UAV technology matures, UAV will become increasingly cost effective, they will grow smaller and be able to accomplish a greater number of missions and fill a greater number of roles. Besides their current applications in Reconnaissance, Surveillance and Target Acquisition (RSTA), the Tactical UAV mission set could be expanded to include target designation,

strike, mine countermeasures, electronic warfare and information warfare. Also as part of the literature review, two in-service tactical UCAVs will be presented.

1. Shadow 200 – AAI Corporation, USA

The Shadow 200 short-range Tactical UAV was developed by AAI Corp. in the 1990s. It has a non-retractable tricycle landing gear for conventional wheeled take-off and landing. The RQ-7A can also be launched from a catapult and has a tailhook to catch arresting cables for a shorter landing strip.

Shadow 200 is capable of spotting targets up to 125 kilometers away from the brigade tactical operations center. It has both day and night capability of identifying tactical vehicles up to 8,000 feet above ground at a slant range of more than 3.5 kilometers. The Shadow ground control station provides near real-time targeting data for precision weapons using “leap ahead” technology and transmits near real time imagery and telemetry data to the end users. The detailed technical specifications are presented in Appendix C. [6]



Figure 4. Shadow 200 being launched from a catapult

2. Watchkeeper Tactical UAV – Thales, UK

The Watchkeeper Tactical UAV system will provide the UK armed forces with Intelligence, Surveillance, Target Acquisition and Reconnaissance (ISTAR) capability. Watchkeeper is a tactical system that will be operated on the battlefield by the British Army Royal Artillery. The air vehicle will be capable of carrying a range of sensors including day and night cameras and surveillance radars. Two WK450 air vehicles will be able to operate in tandem, with the second acting as a communications relay. The ground control station will be network enabled to ensure comprehensive communications links to, for example, airborne stand-off radar, attack aircraft and battlegroup headquarters. The Watchkeeper system will enter service in the British Armed Forces Royal Artillery in 2010. The detailed technical specifications are presented in Appendix D. [7]



Figure 5. Watchkeeper Tactical UAV

III. BUILDING THE PROTOTYPE

A. PROTOTYPE DESIGN

After much research and many reviews have been done on open-source data, it is apparent that there is no commercially available system that can meet the requirements of the proposed KUAV. Therefore, part of this thesis involved the designing and building of the prototype that is capable of integrating with “Rascal” for concept demonstration.

The proposed concept of operations placed many constraints on the design of the KUAV. The three principal considerations for the KUAV are as follows:

Size and weight—It must be small and light so that it can easily integrate with “Rascal”

Lift and drag—It must have high lift and low drag in order to increase the payload and reduce the thrust requirements

Noise signature—The noise signature must be kept to a minimum so that it can have a stealthy approach

With the principal considerations in mind, a non-powered glider with swept linearly tapered wing has been selected as the design for research and experimentation in this thesis.

Due to the tight time schedule, a quick study was conducted on in-service glider systems currently available. The decision was made to design the prototype by scaling down (maintaining an aspect ratio of $AR = 2.78$) the “Swift 2 Wing” hobby flying wing manufactured by Northeast Sailplane Products [8]. Apart from being able to rapidly produce the prototype, the selection of the autopilot was the other important factor. KESTREL™ Autopilot 2.2, manufactured by Procerus Technologies, [9] will be used to control the autonomous flight of the KUAV. This autopilot is being used on a similar

class of test platforms that have tapered wings that are swept linearly. Therefore, this could potentially save much effort and time on tuning the Proportional, Integral and Derivative (PID) gains of the autopilot.

1. Dimensions

Apart from the reasons cited above, the size of the prototype also ensures that it can be easily carried and released without hindering the normal operations of “Rascal.” EH 3.0/12 (3% camber and 12% thick) airfoils, designed by [10], were selected. Table 1 shows the detailed dimensions. Figure 6 shows the plan view of the prototype and the cross section of the airfoil.

Span (mm)	Root Chord (mm)	Taper (%)	Tip Chord (mm)	Sweep (deg)	Area (mm ²)
501.8	203.2	77.6	157.6	34.3	90516

Table 1. Dimensions of prototype

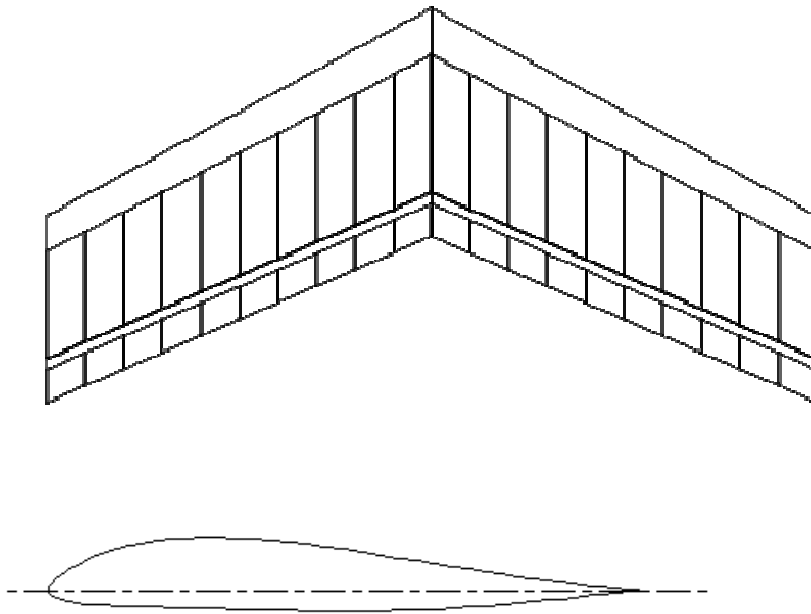


Figure 6. Plan view of prototype and cross section of EH 3.0/12

2. Material

The wing was made from commercial off-the-shelf hobby grade Spyder foam. The foam is durable, lightweight and more importantly, readily available at a low cost. It can be easily cut and shaped using a heated wire. The two main disadvantages of cutting this material (by amateurs) are the surface roughness and the difficulty of shaping a consistent and accurate airfoil shape. They both will decrease lift and increase parasite drag on the airfoil, thus reducing the performance of the airfoil. With these disadvantages in mind, this is still the best solution for rapid prototyping. The elevons of the prototype were made of lightweight balsa wood and the winglets were made of 1/32" aircraft ply.

3. Components and Loading

The prototype was first tested for its aerodynamic performance using a Remote Controlled (RC) flight mode. Only after successful RC flights was the prototype tested for autonomous flight using the Auto Pilot (AP). Different commercial off-the-shelf, hobby-grade components were required for each of these individual flight modes. A detailed breakdown of the components and the respective weight for both modes are presented in Appendix E.

4. Trimming and Balancing

The theoretical aerodynamic center of the prototype was estimated to be at 25% of the Mean Aerodynamic Chord (*MAC*) computed using equation (1).

$$MAC = rc \times \frac{2}{3} \times \frac{(1+t+t^2)}{(1+t)} \quad (1)$$

where rc = Root Chord and t = Taper Ratio

MAC was computed to be 181 mm and the theoretical aerodynamic center is located at 128 mm on the root chord from the nose. After balancing all the components and trimming from hand-launched RC test flights, the optimum center of gravity CG was

found to be located at approximately 118 mm from the nose on the root chord resulting in a static margin of 10 mm. The details are depicted in Figure 7.

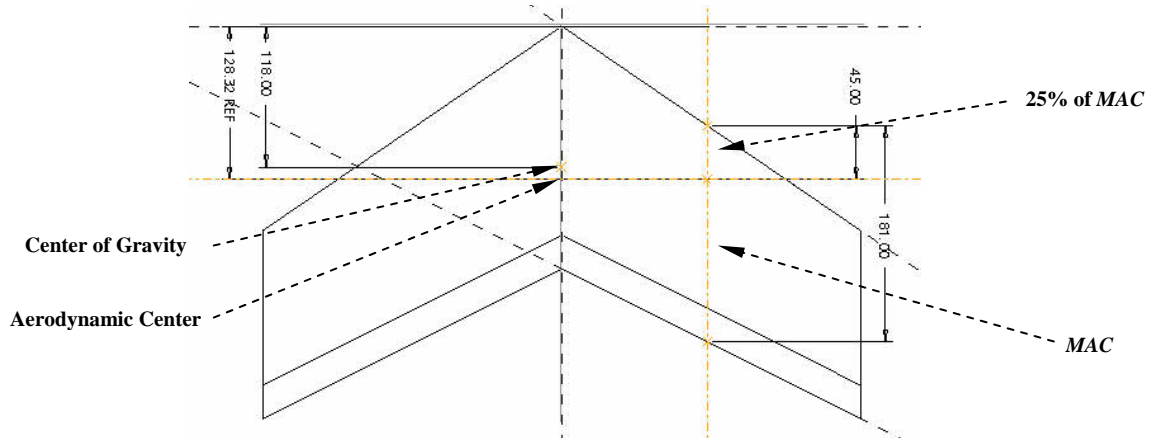


Figure 7. Location of aerodynamic center and CG

Since this static margin is already sufficient for trim flight during hand-launched test flights (low altitude and short duration). The author is confident that the prototype KUAV will exhibit more stable performances during “Rascal” launched test flights (high altitude and long duration).

5. Completed Prototype

The main components (from left to right: autopilot, battery-pack, GPS and modem) used for the autonomous flight are shown in Figure 8.



Figure 8. Components for autonomous flight

The prototype KUAV is shown Figure 9. The components described above except the GPS, will be packed in an opening cut on the airfoil under the plastic cover shown in Figure 9. A separate slot will be cut on the airfoil to house the GPS unit.

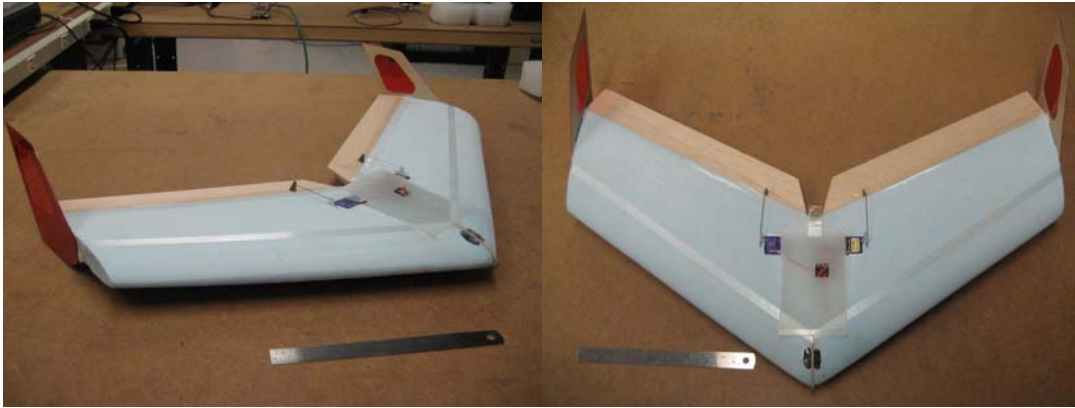


Figure 9. Side and top views of the prototype KUAV

THIS PAGE INTENTIONALLY LEFT BLANK

IV. AERODYNAMICS STUDIES

A. BASIC AERODYNAMICS FOR GLIDERS

The aerodynamic forces acting on a non-powered glider closely resemble those on any aircraft. The key distinction is that the non-powered glider does not produce thrust force to counteract the drag force. As a result, a glider cannot maintain a level flight at constant speed and altitude. A glider in steady gliding flight is always descending relative to the air around it. The glider is essentially trading altitude to maintain its velocity. Figure 10 shows the balance of forces acting on a glider descending in a steady glide at constant velocity.

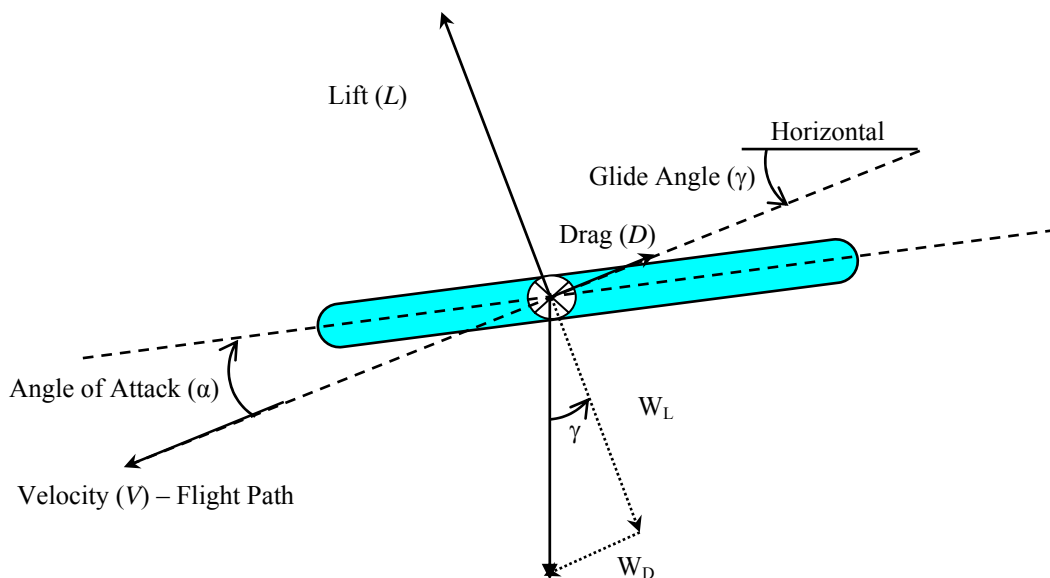


Figure 10. Forces acting on a glider in flight

The glider follows a path that slopes at an angle below horizontal called the Glide Angle, denoted by the Greek letter (γ). The direction of the glider's motion along the glide path is shown by the velocity arrow on the diagram. (Note that the glider's longitudinal axis is not pointing along the direction of motion, but slightly above the glide path at angle α , called the Angle of Attack, AOA).

The lift force (L), which according to linear theory acts at a right angle to the velocity through the air, is tilted forward from vertical at an angle equal to γ . Drag (D) acts directly opposite the direction of motion through the air.

At trim condition (constant glide angle and velocity) the following relationships can be derived.

$$L = W_L \rightarrow L = mg \cos \gamma \quad (2)$$

$$D = W_D \rightarrow D = mg \sin \gamma \quad (3)$$

It can be observed that when all forces on the glider are balanced there is no net force to cause acceleration, so the glider will move along the glide slope at a constant velocity. The velocity (V) and glide angle (γ) can be derived from equations (2) and (3) respectively.

$$L = \frac{1}{2} \rho AV^2 C_L \quad \text{and} \quad D = \frac{1}{2} \rho AV^2 C_D$$

$$\therefore \frac{1}{2} \rho AV^2 C_L = mg \cos \gamma \quad (4)$$

$$\therefore \frac{1}{2} \rho AV^2 C_D = mg \sin \gamma \quad (5)$$

$$\tan \gamma = \frac{C_D}{C_L} \rightarrow \gamma = \tan^{-1} \frac{C_D}{C_L} \rightarrow \gamma = \tan^{-1} \frac{D}{L} \quad (6)$$

$$V = \sqrt{\frac{2mg}{\rho A (C_L \cos \gamma + C_D \sin \gamma)}} \quad (7)$$

B. SIMULATION USING ANALYTICAL TECHNIQUES

Commercial off-the-shelf software, *LinAir* (Version 4.3) [11] was used in this thesis to analyze the aerodynamic characteristics of the glider. *LinAir* is a linear panel code program capable of computing aerodynamic characteristics of multi-element, nonplanar lifting surfaces for a given wing geometry and angle of incidence. The results

generated are based on solving the Prandtl Glauert linear partial differential equations for inviscid, irrotational and subsonic flow.

1. Verification of Panel Codes

There is a need to first “calibrate” several input parameters to *LinAir*, so that the results generated can be benchmarked with existing wind tunnel results for a similar class of wing profile. This is especially true for cambered airfoil, as the procedures for modeling airfoil with camber stated in [11] are strictly adhered to. It was found that EH3.0/12 has zero lift at AOA of approximately -1° . Therefore, all results generated will be adjusted by adding -1° to the actual incidence angle.

In the proposed operating envelope of the glider (low altitude and low speed) the Reynolds Number (Re) is expected to fall in the region of 50,000 to 100,000. Wind tunnel experimental results obtained by [12] provide a good insight into the aerodynamic performance of low aspect ratio wings at low Re . This served as an excellent independent source to cross-check the data generated by *LinAir*.

Many aerodynamic parameters, in particular those related to drag, cannot be computed analytically or by linear methods and are even difficult to get right using Navier-Stokes solvers, and are usually obtained from wind tunnel experiments. Extensive tests for wings of $AR = 1$ and 2 at $Re = 70,000$ and $100,000$ have been conducted and the results are presented in [12]. In the absence of wind tunnel facilities and time, the following parameters, Drag Coefficient at Zero Lift (C_{D_0}) and Induced Drag Coefficient (K) for the prototype glider ($AR = 2.78$) will be inferred based on the results published by [12].

It is assumed that the total drag produced by a wing is give by equation (8). The values of C_{D_0} and K can be obtained by plotting C_D vs. C_L^2 for each model and applying a least-square linear regression to the data. The wind tunnel data obtained by [12] are summarized in Table 2.

$$C_D = C_{D_0} + KC_L^2 \quad (8)$$

AR	CD0	K
1	0.015	0.5
2	0.020	0.4

Table 2. Wind tunnel results of C_{D_0} and K for wings of AR 1 and 2

These data were subsequently run on *LinAir* using wing profiles matching the respective AR . The results generated for $AR = 2$ (AOA from 0° to 10°) closely matched those obtained in the wind tunnel. However, for $AR = 1$, *LinAir* produced a better match using $K = 0.4$. The detailed results are presented in Appendix F.

Since the prototype has an AR of 2.78, by extrapolating from the above simple verification, $C_{D_0} = 0.022$ and $K = 0.4$ will be used to model the prototype glider. *LinAir* has proven to be suitable and will be used as the analytical tool for estimating the aerodynamic performance of the prototype.

2. Geometry and Input File

The geometry of the glider described in Chapter III was modeled using a total of 40 panels covering the entire wing surface and the two elevons as shown in Figure 11. The input file is shown in Appendix G.

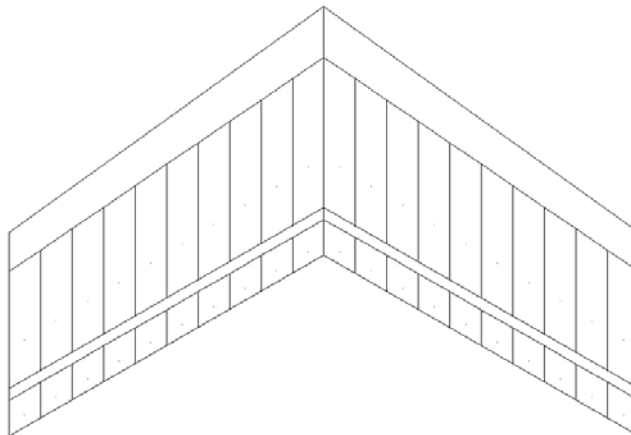


Figure 11. Geometry of glider generated by *LinAir*

3. Aerodynamic Data

The aerodynamic performance of the glider was evaluated for AOA from 0° to 20° at an interval of 0.5° . (This range of AOA is only feasible for ideal linear theory simulations using *LinAir*. The operating AOA range is expected to be lower in practical model and physical implementation.) Negative AOA were not examined as it is not possible to maintain steady flight for negative AOA for a non-powered glider. More importantly, it does not contribute to any performance improvement. Numerical results generated by *LinAir* for both the non-cambered airfoil and with the adjustments made for the cambered airfoil are shown in Appendix H.

C. ANALYTICAL TRADEOFF STUDIES

Three main performance parameters of the glider were examined.

Glide Velocity (V)

Horizontal Range (R)

Airborne Endurance (E)

These performance parameters are also functions of AOA and γ . Using the data generated, the following five tradeoff studies were analyzed at a release altitude of 300 m which is a typical operating ceiling for tactical systems.

Tradeoff Study 1 - L/D vs. AOA

Tradeoff Study 2 - γ vs. L/D

Tradeoff Study 3 - R vs. L/D

Tradeoff Study 4 - V vs. AOA

Tradeoff Study 5 - E vs. V

1. Tradeoff Study 1 - L/D vs. AOA

It is important to recall at this juncture that the values of L used in this analysis are estimated by *LinAir*. *LinAir* is a linear panel code program, it assumes that L always

varies linearly for all AOA and does not include the effects of flow separation and stall which are dominant at higher AOA . Conversely, the effects of flow separation and stall are approximated in D , as D is a quadratic curve fit to empirical data. (The plot showed in Figure 12 will change if L is computed accurately with considerations to the effects of flow separation and stall.)

This study is confined to the region of AOA around 3° to 6° where the effects of flow separation and stall are negligible. Therefore, the results presented in Figure 12 in the region of AOA around 3° to 6° are valid to this study.

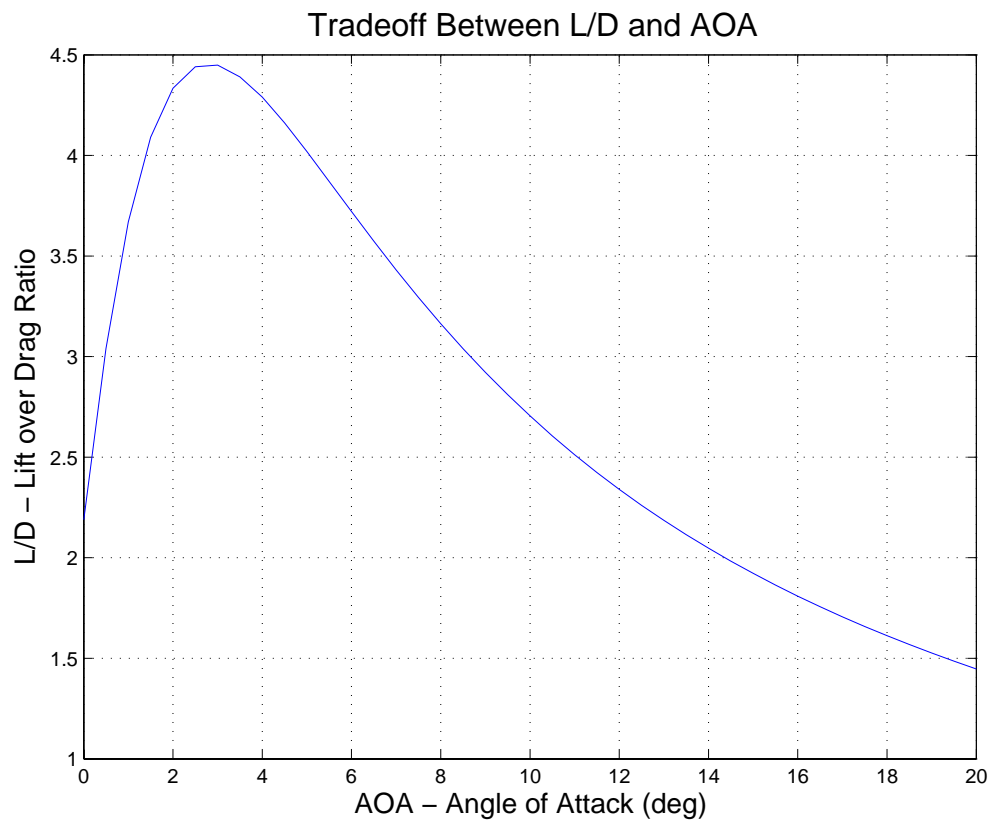


Figure 12. Tradeoff between L/D and AOA

Analysis of Figure 12 shows that the maximum L/D of approximately 4.4 occurred at an AOA of 3° . The data presented in Table 3 shows the comparison between the analytical results to those obtained by [12] through wind tunnel experiments.

Experimental Wind Tunnel Data				
S/No	AR	L/D	AOA	Re
1	1.00	4.8	6.0°	70,000
2	2.00	5.0	4.0°	70,000
Analytical LinAir Result				
3	2.78	4.4	3.0°	70,000

Table 3. Comparison between experimental and analytical results

The above comparison shows that the results obtained from *LinAir* are comparable to the wind tunnel experiment and the selected values of $C_{D_0} = 0.022$ and $K = 0.4$ are within acceptable engineering estimates.

2. Tradeoff Study 2 – γ vs. L/D

It was shown in Equation (6) that γ is a function of L/D . The greater the L/D , the gentler the glide slope will be and vice versa. This result is shown in Figure 13.

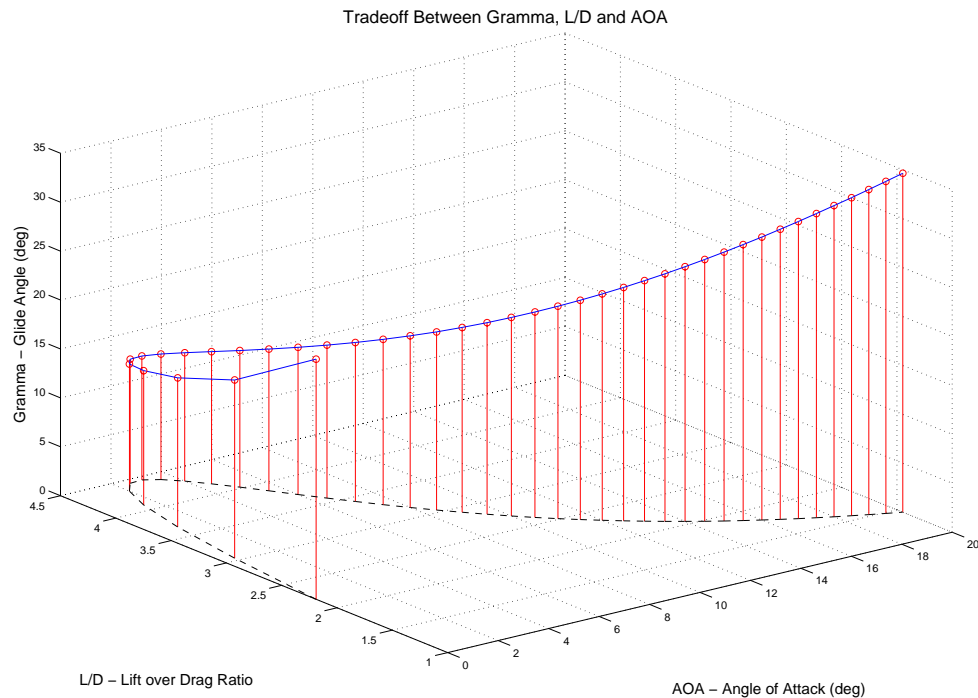


Figure 13. Tradeoff between γ , L/D and AOA

The graph of Tradeoff Study 1 was projected on the x-y plane and the z-axis shows the values of γ with varying AOA and L/D .

Therefore, following the results of Tradeoff Study 1 and the relationship presented in equation (6), γ would first decrease with increasing AOA . After stall condition, γ would increase with increasing AOA . A minimum glide angle of 12.7° would occur at the AOA of 3° where L/D was at the maximum.

3. Tradeoff Study 3 – R vs. L/D

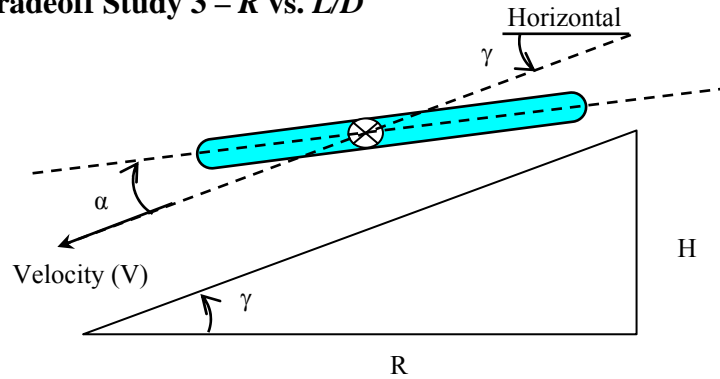


Figure 14. Glide path geometry

The glide path shown in Figure 14 can be related through equation (9). The gentler the glide slope (smaller γ), the farther the glider will travel horizontally before reaching the ground. Therefore, maximum R will occur at minimum γ .

$$\tan \gamma = \frac{H}{R} \rightarrow R = \frac{H}{\tan \gamma} \quad (9)$$

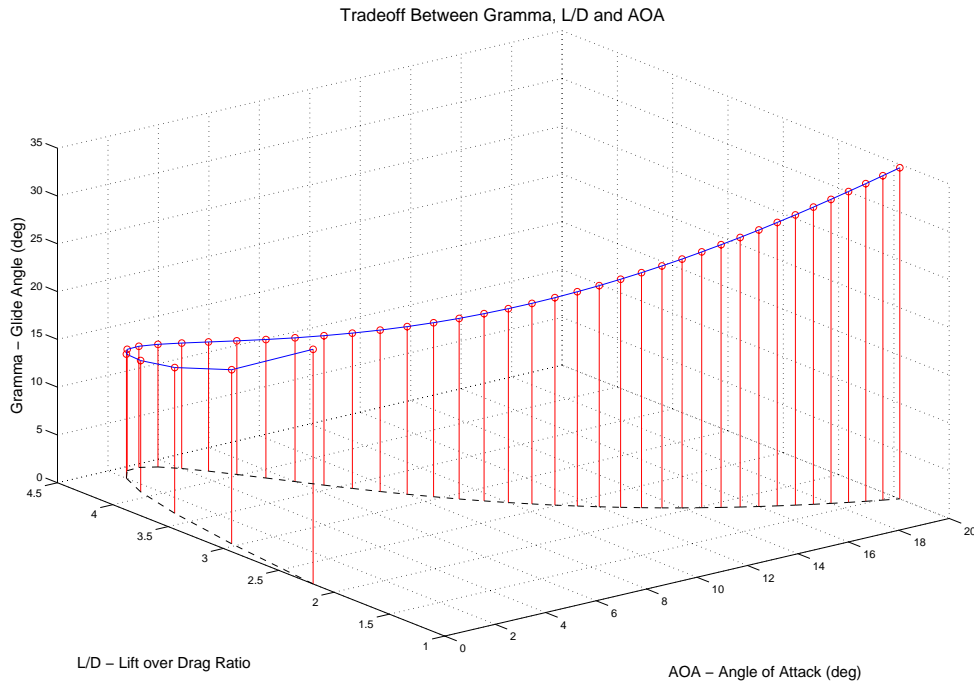


Figure 15. Tradeoff between R , L/D and AOA

The result of maximum R occurring at minimum γ is shown in Figure 15. The graph of Tradeoff Study 1 was again projected on the x-y plane and the z-axis shows the values of R with varying AOA and L/D .

Therefore, following the results of Tradeoff Study 1 and 2 and the relationship presented in equation (9), R would first increase with increasing AOA . After stall condition, γ would decrease with increasing AOA . A maximum R of approximately 1.335 km would occur at the AOA of 3° where γ is at the minimum and L/D is at the maximum.

4. Tradeoff Study 4 – V vs. AOA

It has been explained that a non-powered glider does not produce thrust to counter drag. In order to maintain a trimmed glide path, it is always trading off altitude to maintain its velocity. Equation (7) shows the analytical expression of the glide velocity at trimmed flight with a fixed AOA .

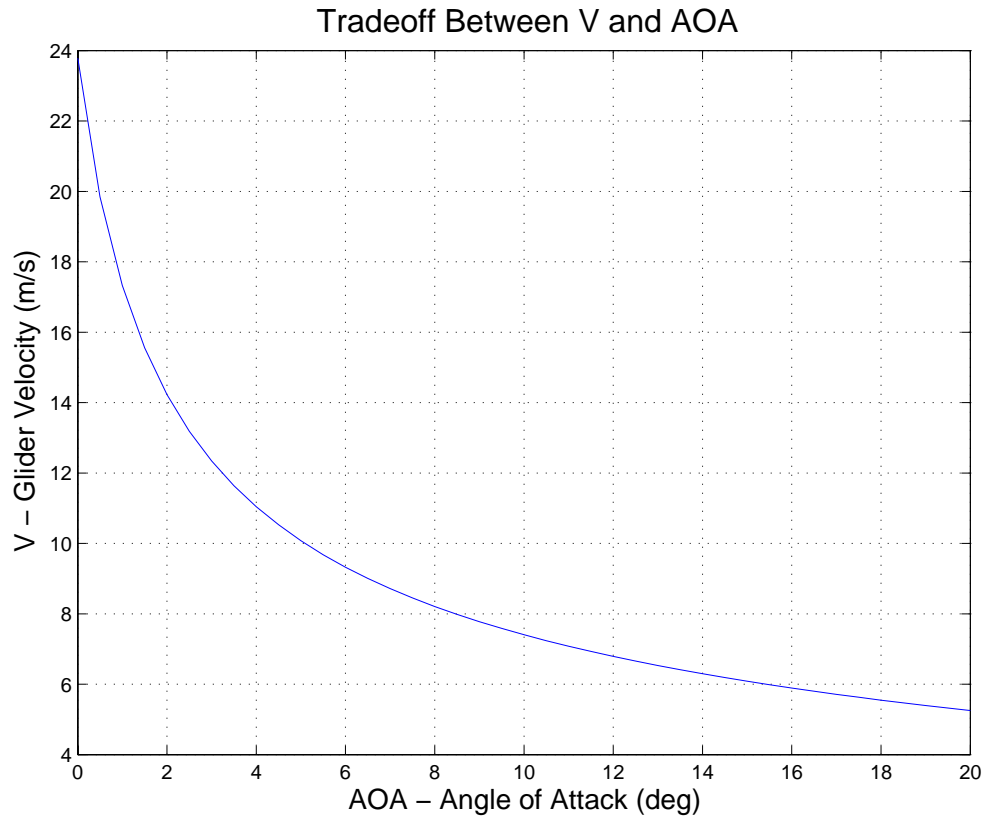


Figure 16. Tradeoff between V and AOA

Analysis of Figure 16 shows that V increases exponentially at low AOA and decreases gradually at high AOA . This behavior of V is critical to the next tradeoff study where speed is varied to achieve the desired airborne endurance.

5. Tradeoff Study 5 – E vs. V

Trimming the glider to fly at its maximum L/D will allow it to fly farthest horizontally, but it will not result in the longest airborne endurance (E) (duration of time in the air).

E depends on the vertical sink rate, or rate of decrease in altitude (H), as shown in equation (10). This depends on both the glide angle and the glide speed. Maximum E is achieved by trimming the glider to fly at an AOA higher than that where maximum L/D occurs. (L/D will decrease slightly from the maximum value.) This will result in a steeper

glide slope, but it will cause a significant reduction of glide velocity. The reduction in speed is sufficient to compensate for the effects of the steeper glide slope that are needed to achieve maximum E .

$$E = \frac{H}{V_y} \quad \text{where} \quad V_y = V \sin \gamma \quad (10)$$

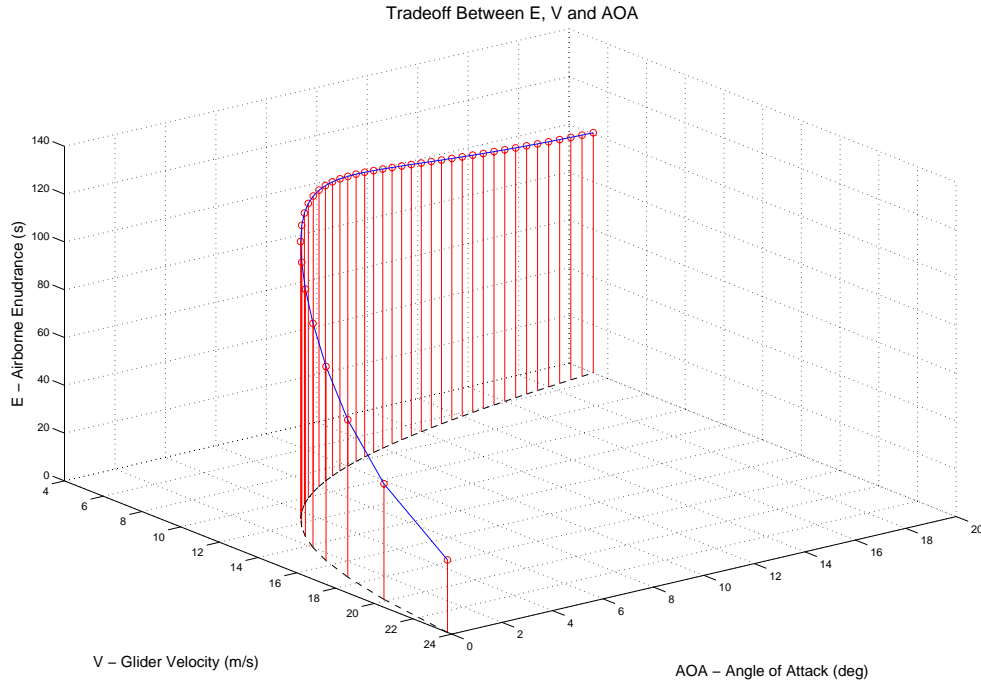


Figure 17. Tradeoff between E , V and AOA

Maximum E is achieved by trimming the glider to fly at a higher AOA , and this result is shown in Figure 17. The graph of Tradeoff Study 4 was projected on the x-y plane, and the z-axis shows the values of E with varying AOA and V .

Therefore, following the results of Tradeoff Study 4 and the relationship presented in equation (10), E would first increase with increasing AOA until slightly after maximum L/D condition. Following maximum L/D condition, E would decrease with

increasing AOA because a decrease in speed is insufficient to compensate for the effects of the increasing glide angle. A maximum E of approximately 124 s would occur at the AOA of 6° .

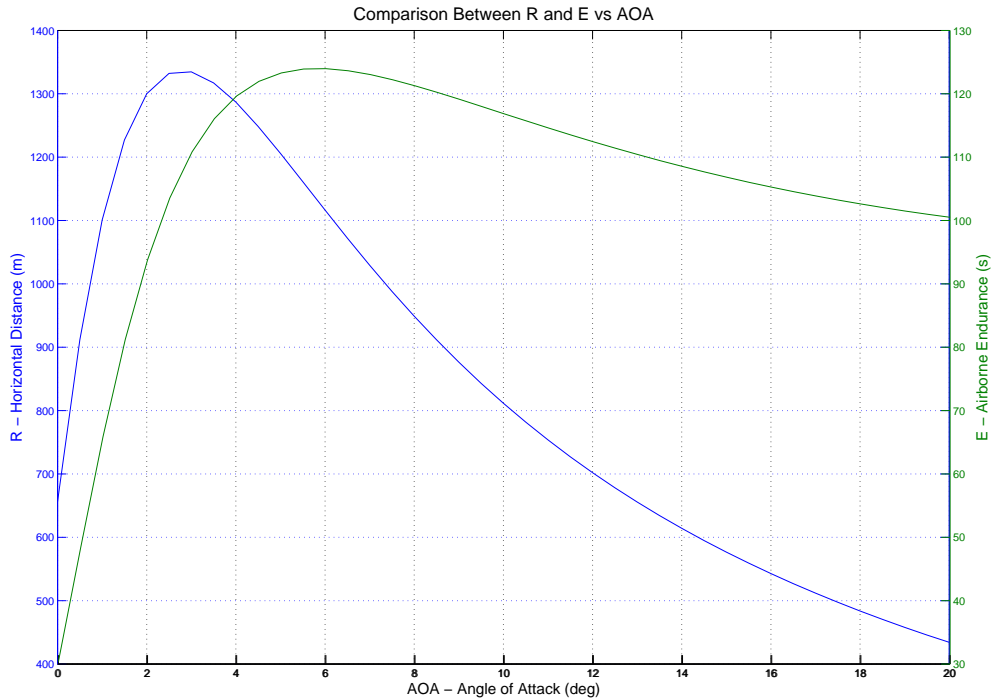


Figure 18. Comparison between R and E vs. AOA

Finally, it can be concluded from the analysis of Figure 18 that maximum R occurs at an AOA of 3° where L/D is the maximum. Maximum E occurs at a slightly higher AOA of 6° where further reduction in speed is sufficient to compensate for the effects of the steeper glide slope. Maximum E can only be achieved at the expense of horizontal distance (approximately 16.5% reduction in R).

The results obtained from the above theoretical tradeoff studies under ideal operating conditions will define the most optimistic operational envelope of the prototype KUAV. The tradeoff between critical performance parameters provides a basis for the end-user to plan for different engagement scenarios like long range (where maximum range is desired), loiter (where high endurance is desired) and dash (where high speed is

desired). In Chapter V, the operational envelope of the prototype KUAV will be examined under practical operating conditions. These conditions will be modeled as closely as possible using numerical methods (MATLAB Simulink).

THIS PAGE INTENTIONALLY LEFT BLANK

V. GUIDANCE AND CONTROL

A. SIMULATION USING NUMERICAL TECHNIQUES

The analysis of the aerodynamic performance data generated by *LinAir* was based purely on analytical closed-form solutions derived from equations of motions. These ideal conditions can never be replicated in practical implementations. The actual performance of the prototype will be dependent on many other factors such as sensor measurement errors, variations in atmospheric conditions, the performance of the autopilot and control algorithm and the efficiency of the mechanical devices onboard.

It is almost impossible to simulate the exact operating environment with current technology, in particular for conditions involving low Re where variations in aerodynamic behaviors and performances are highly non-linear. However, there is still an absolute need to account for as many imperfections as possible in order to better estimate and predict the operational envelope of the prototype KUAV. MATLAB Simulink and the aerodynamic performance data generated by *LinAir* will be utilized to model a more realistic operating environment for the prototype.

This process is summarized in Figure 19.

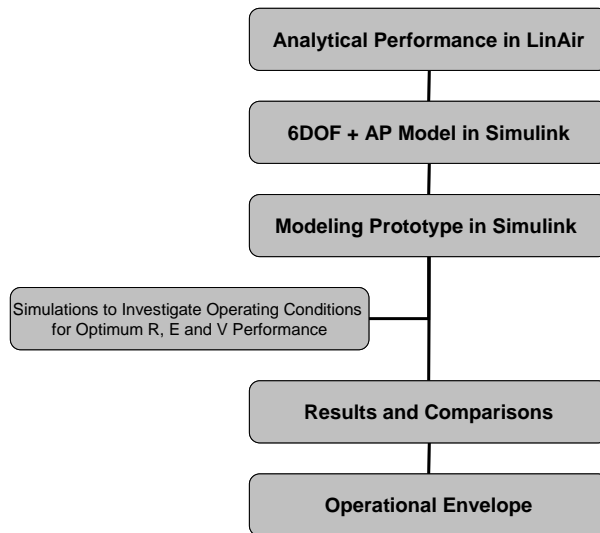


Figure 19. Flow chart depicting simulation process

1. Analytical Results from *LinAir*

Chapter III illustrated how the results generated by *LinAir* were used to investigate the aerodynamic performance of the prototype based on analytical equations of motions in ideal operating conditions. These dimensionless coefficients from *LinAir* will be used to define the aerodynamic performance of the prototype in the model described below.

2. 6 Degree of Freedom (DOF) + Auto Pilot (AP) Simulink Model

An existing Simulink Model for Silver Fox UAV previously developed by [13] has been used to model the performance of the prototype. A straightforward modification was made to the model to more closely approximate the configuration of the prototype KUAV. The engine was removed from the model because the non-powered glider does not produce thrust. The modified model is shown in Figure 20. It is comprised of the following three main blocks: the AP Inner loop, Forces and Moments and the 6DOF equations of motion.

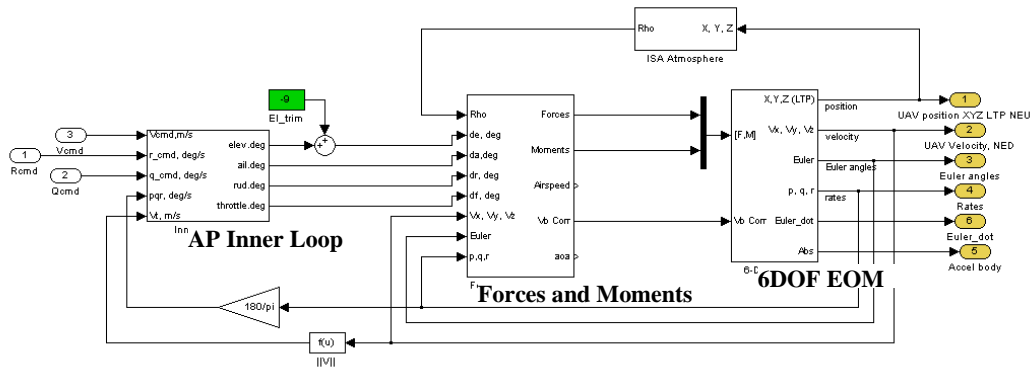


Figure 20. Simulink Block Diagram for 6DOF + AP Model

The 6DOF EOM block implements the equations for a constant-mass rigid-body 6DOF aircraft with respect to the body frame $\{B\}$. The detailed derivations will not be presented in this thesis as they can be found in [14]. In summary, the motions of a 6DOF aircraft can be completely described by the following set of equations:

Linear Momentum Equation

$${}^B\bar{F} = m\left({}^B\bar{v} + {}^B\bar{\omega} \times {}^B\bar{v}\right)$$

Angular Momentum Equation

$${}^B\bar{G} = J {}^B\bar{\omega} + {}^B\bar{\omega} \times (J {}^B\bar{\omega})$$

Euler Equations relating body rates and attitudes angles

$$\dot{\phi} = p + q(\sin \phi + r \cos \phi) \tan \theta$$

$$\dot{\theta} = q \cos \phi - r \sin \phi$$

$$\dot{\psi} = \sec \theta (q \sin \phi + r \cos \theta)$$

The Forces and Moments block implements the forces and moments acting on the prototype due to aerodynamics and gravitational effects. They can be expressed as:

$$\begin{bmatrix} {}^B\bar{F} \\ {}^B\bar{G} \end{bmatrix} = \begin{bmatrix} {}^B\bar{F}_{aero} + {}^B\bar{F}_{grav} \\ {}^B\bar{G}_{aero} \end{bmatrix}$$

For simplicity, the aerodynamic forces and moments acting on the aircraft are often defined in terms of dimensionless aerodynamic coefficients that are functions of the deflections of the control surfaces.

$$\begin{bmatrix} {}^B\bar{F}_{aero} \\ {}^B\bar{G}_{aero} \end{bmatrix} = qS \begin{bmatrix} {}^B_w R \begin{bmatrix} C_D \\ C_Y \\ C_L \end{bmatrix} \\ {}^B_w R \begin{bmatrix} C_l b \\ C_m c \\ C_n b \end{bmatrix} \end{bmatrix}$$

Where q is the dynamic pressure and S is the wing reference area.

${}^B_w R$ is the transformation matrix that rotates a vector from the wind coordinate frame to the aircraft body frame.

The numerical values for the dimensionless aerodynamics coefficients were determined from the data generated by *LinAir*. The detailed explanation will be presented in the next section.

The gravitational forces acting on the rigid body will not generate moments as they are assumed to be acting on the center of gravity.

$${}^B\bar{F}_{grav} = {}^B_L R \begin{bmatrix} 0 \\ 0 \\ mg \end{bmatrix}$$

${}^B_L R$ is the rotation matrix that rotates a vector from the earth frame to the aircraft body frame.

In summary, the forces and moments acting on a 6DOF aircraft can be completely described by the following equations.

$${}^B\bar{F} = qS {}^B_L R \begin{bmatrix} C_D \\ C_Y \\ C_L \end{bmatrix} + {}^B_L R \begin{bmatrix} 0 \\ 0 \\ mg \end{bmatrix}$$

$${}^B\bar{G} = qS {}^B_L R \begin{bmatrix} C_l b \\ C_m c \\ C_n b \end{bmatrix}$$

Finally, the AP Inner Loop block implements the inner loop of the autopilot developed by [13].

3. Modeling the Prototype KUAV in the 6DOF + AP Model

There is a need to initialize the 6DOF + AP model at the operating conditions and performance of the prototype KUAV. This initialization process is critical so that the model will generate accurate results based on realistic operating conditions and aerodynamic performance of the prototype KUAV. As mentioned in the previous section, the dimensionless coefficients obtained from *LinAir* will be used to model the aerodynamic performance of the prototype.

The initialization script file of the model is shown in Appendix I. The coefficients of performance under the ‘‘Aerodynamic Derivatives’’ are initialized using the data generated by *LinAir* (units of per radian). The following approximating relationships are used to compute the coefficients:

$$C_D = C_{D0} + A_1 C_L + A_2 C_L^2$$

$$C_Y = C_{Y\beta} \beta + C_{Y\delta r} \delta r$$

$$C_L = C_{L0} + C_{L\alpha} \alpha + C_{L\dot{\alpha}} \dot{\alpha} + C_{L\delta e} \delta e + \frac{C_{Lq} q}{|B\vec{v}|}$$

$$C_l = C_{l\beta} \beta + C_{l\delta a} \delta a + C_{l\delta r} \delta r + \frac{b}{2|B\vec{v}|} (C_{lp} p + C_{lr} r)$$

$$C_m = C_{m0} + C_{m\alpha} \alpha + C_{m\dot{\alpha}} \dot{\alpha} + C_{m\delta e} \delta e + \frac{C_{mq} qc}{|B\vec{v}|}$$

$$C_n = C_{n\beta} \beta + C_{n\delta e} \delta e + C_{n\delta r} \delta r + \frac{b}{2|B\vec{v}|} (C_{np} p + C_{nr} r)$$

Where $\delta e, \delta a, \delta r$ represent the deflection of the elevator, aileron and rudder respectively. (As the prototype KUAV is designed to be a flying wing, there is no rudder and the elevons function as both elevators and ailerons. $\delta r = 0$ and $\delta e = \delta a$.)

p, q, r are the angular rates, b is the wing span, c is the mean aerodynamic chord and α and β represent the angle of attack and the sideslip angle respectively.

4. Simulation Procedures

In all realistic non-linear models, huge amount of transient response is often expected which is detrimental to the accuracy of the results generated. It is important to note at this point, that only the results from the steady-state conditions, better known as trim conditions, will be used for analysis. Therefore, there is a need to minimize the duration of this transient response. This is achieved by running the simulation with the

initial conditions as close to the trim conditions as possible. This will greatly improve the accuracy of the results obtained from the simulations.

Specifically for this study, it has already been shown that the performance of the non-powered glider depends on the trim conditions. This is primarily determined by the glider's *AOA* which in turn is controlled by the deflection of the elevators. Therefore, it is necessary to ensure that the initial conditions, with respect to the body frame, correspond to trim conditions. The following procedures were adopted for this study:

The Linearization Task function in Simulink Control Design Blockset was used to obtain the steady-state velocity for every 1° change in elevator deflection. It was found in this step that steady-state conditions could only be achieved for *AOA* between 1° and 8° . This operating range of *AOA* is significantly smaller than those used in Chapter IV. This is expected as *LinAir* is programmed based on linear theory (linearized solution does not diverge) and it will generate results even for an *AOA* of 90° .

The body velocity in the initialization script file was set to the corresponding trim conditions of the respective *AOA*. (This is to minimize the transient response and improve the accuracy of the simulation results.)

The model was run for *AOA* from 1° to 8° .

The output from the workspace for Range (x-position), Velocity and Endurance (time) was saved when the altitude (z-position) reached zero.

The results of the simulations for a release altitude of 300m are attached in Appendix J.

5. Results and Comparisons

The results obtained from the 6DOF + AP model were compared to the results found in the ideal operating environment (presented in Chapter III).

Comparison Between Analytical and 6DOF + AP Models for L/D vs. AOA

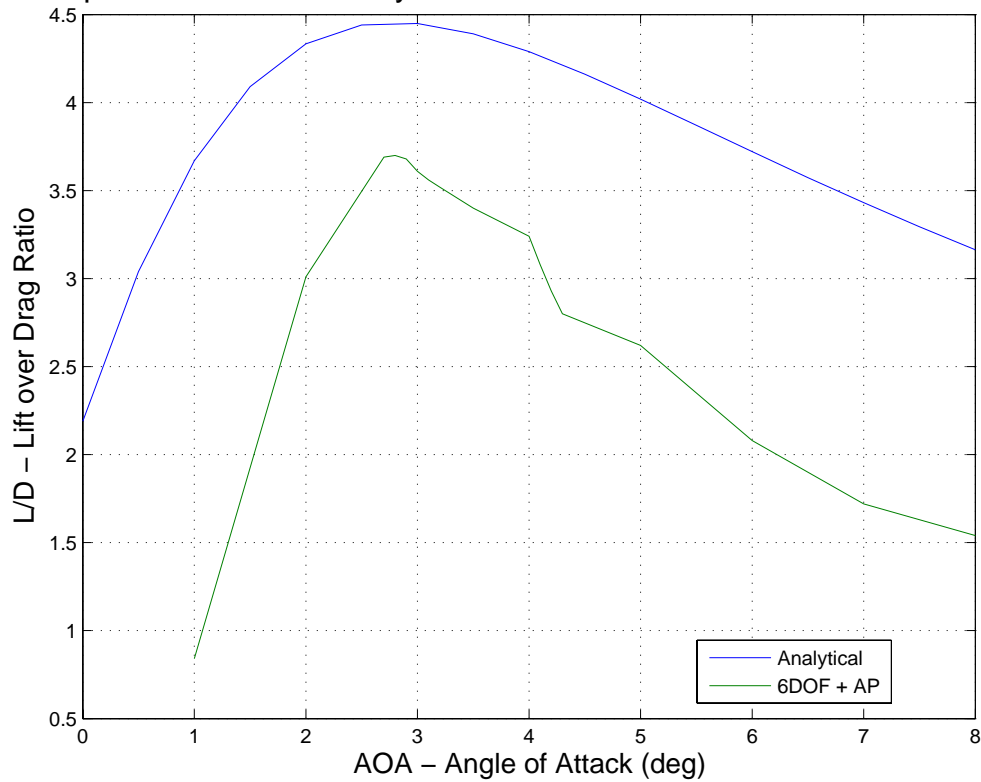


Figure 21. Comparison between analytical and 6DOF + AP models for L/D vs. AOA

Analysis of Figure 21 shows that the L/D of the 6DOF + AP model is about 16% lower than the L/D obtained in the analytical model. This result was expected, as imperfections in practical environments will reduce the performance of any system.

Maximum $L/D = 4.4$ at $AOA = 3.0^\circ$ (Analytical model)

Maximum $L/D = 3.7$ at $AOA = 2.8^\circ$ (6DOF + AP model)

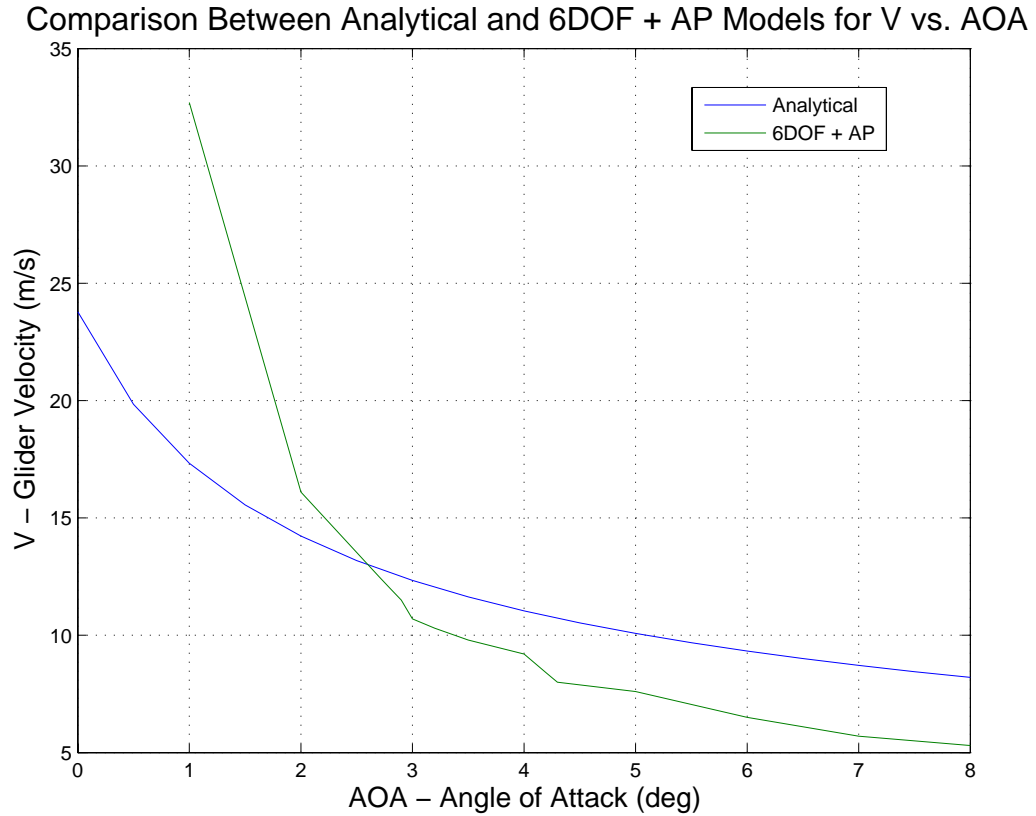


Figure 22. Comparison between analytical and 6DOF + AP models for V vs. AOA

Analysis of Figure 22 shows that the change in V with increasing AOA exhibits the same behavior in the 6DOF + AP model as the analytical model. In the region ($AOA < 2.5^\circ$) where V decreases exponentially, system imperfections caused the glider to travel at a higher speed. In the region ($AOA > 2.5^\circ$) where V decreases gradually, system imperfections caused the glider to travel at a lower speed.

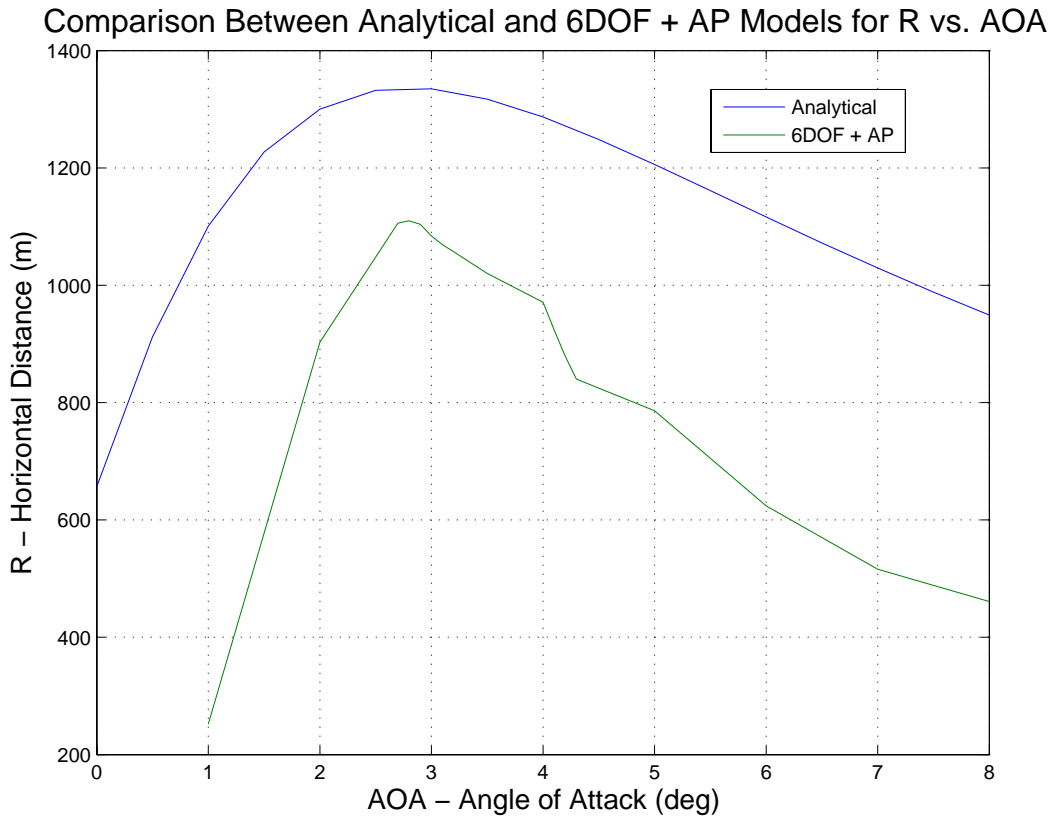


Figure 23. Comparison between analytical and 6DOF + AP models for R vs. AOA

Analysis of Figure 23 shows that the R generated from the 6DOF + AP model is about 17% lower than the R obtained from the analytical model.

Maximum $R = 1.335$ km at $AOA = 3.0^\circ$ (Analytical model)

Maximum $R = 1.110$ m at $AOA = 2.8^\circ$ (6DOF + AP model)

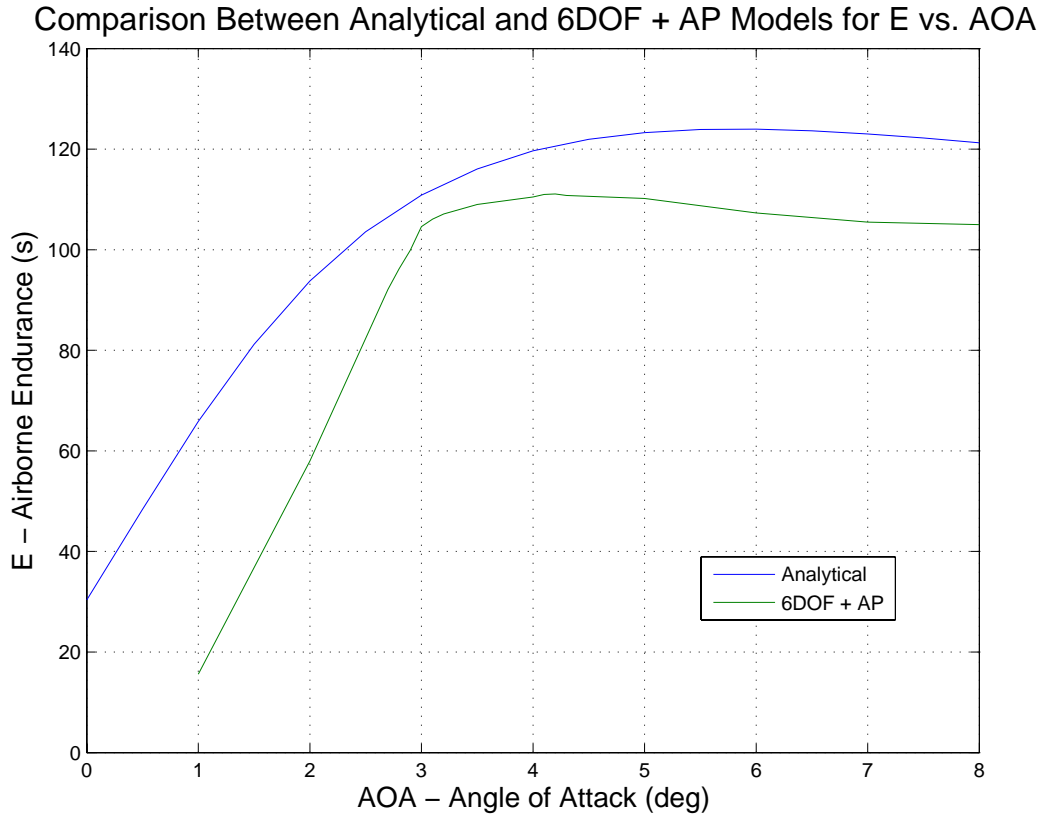


Figure 24. Comparison between analytical and 6DOF + AP models for E vs. AOA

Analysis of Figure 24 shows that the practical E is about 10% lower than the E obtained in an ideal environment.

Maximum $E = 124$ s at $AOA = 6.0^\circ$ (Analytical model)

Maximum $E = 111.1$ s at $AOA = 4.2^\circ$ (6DOF + AP model)

6. Refinement of Operational Envelope

It was mentioned in Chapter IV that the results obtained from *LinAir* predict the most optimistic (upper bound) operational envelope of the prototype KUAV. The results obtained from the 6DOF + AP model in this simulation predict the most conservative (lower bound) operational envelope.

The maximum horizontal range where the prototype can travel (with a release altitude of 300 m) is 1.11 km at an *AOA* of 2.8° . Alternatively, it can sacrifice range to achieve a maximum airborne endurance of 111 s at an *AOA* of 4.2° .

The actual performance of the prototype KUAV should fall within the upper and lower bound predicted by the analytical and the 6DOF + AP model respectively. Prior to the physical test flight, it is of great importance to conduct the hardware-in-the-loop (HIL) experiments to predict the actual performance of the prototype KUAV. The HIL procedures and results are presented in Chapter VI.

THIS PAGE INTENTIONALLY LEFT BLANK

VI. HARDWARE-IN-THE-LOOP EXPERIMENTS

A. ARCHITECTURE AND SETUP

Due to the tight timeline of this research, there is no means for the author to develop a new guidance law to provide reference commands to the autopilot inner loop. This is similar to the AP Inner Loop block described in Chapter V. Therefore, COTS Kestrel Autopilot is selected as the hardware for autonomous flight. Its default GPS waypoint navigation algorithm will be utilized to provide guidance reference commands to the autopilot inner loop.

The next step to perform is hardware-in-the-loop (HIL) experiments using the physical autopilot hardware. These will verify the results obtained in analytical and numerical analysis done prior to actual test flight. Kestrel Autopilot and Virtual Cockpit have a built-in ability to simulate a 6DOF UAV through the use of a 3rd party, open-source simulator called Aviones. Aviones displays the simulated flight in 3D space, which allows the user to quickly and easily visualize the flight plans.

This is the first attempt by the team to set up HIL for Kestrel Autopilot. Therefore it is important that the system architecture, set up and experimentation procedures are properly documented for knowledge retention.

1. Architecture

There are two options available for setting up the HIL. A brief summary of each option is presented. The detailed descriptions are found in the Kestrel Users Guide [15].

Architecture 1, which uses a TCP/IP connection as shown in Figure 25.

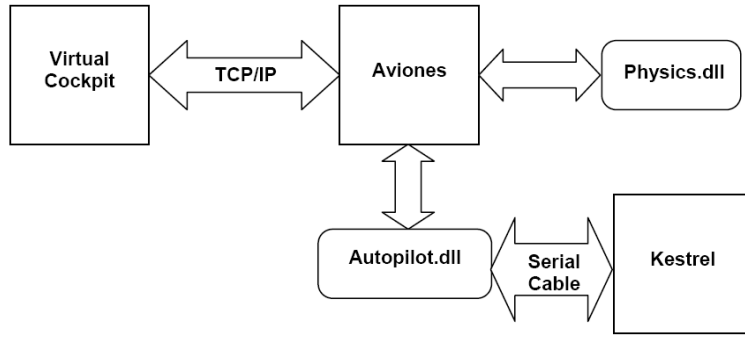


Figure 25. HIL architecture using a TCP/IP connections

In the TCP/IP architecture, Virtual Cockpit communicates with Aviones over a TCP/IP connection. Aviones passes data (body rates and body velocities) from Virtual Cockpit to the autopilot over a hardwired serial connection. The practical advantage of this method is that only one serial port is needed (which is the configuration for most laptop in the current market). The disadvantage is that the modem needs to be unplugged from the autopilot and the results obtained will not account for any latency due to data transmission by the modem.

Architecture 2 which uses a standard serial modem interface as shown in Figure 26.

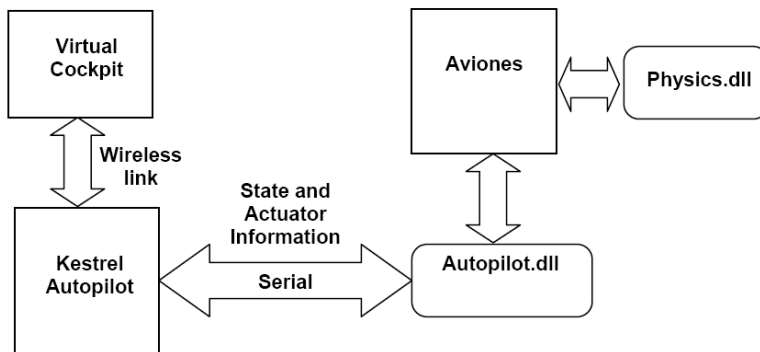


Figure 26. HIL architecture using a standard serial modem interface

In the serial modem architecture, the autopilot communicates with Virtual Cockpit over the standard serial modem interface. Aviones communicates with the autopilot over a serial connection. The advantage of this method is that the modem will be left connected to the autopilot as per actual operating configuration. The results

obtained will give a more accurate representation of the predicted performance. The main disadvantage of this set up is that the user will be exposed to unnecessary radiation emitted from the commbox.

Weighing between the advantages and disadvantages of the two options and hardware availability, Architecture 1 was selected for this research.

2. Setup

In this thesis, the TCP/IP architecture was setup for the HIL experiments. The details procedures are presented in Appendix K.

Additional lessons learned by the author are also documented for future reference.

When future studies are done, the most current version of Virtual Cockpit Aviones must be loaded. (At the time of this experiment, the latest software versions were Virtual Cockpit, version 2.4.2 and Aviones, version 2007-11-1)

When using Virtual Cockpit, version 2.4.2, an update for Microsoft DirectX must be installed. The update can be downloaded from <http://www.microsoft.com/windows/directx/default.mspx>

The most current version of the firmware for the autopilot must be programmed into the autopilot hardware. (At the time of this experiment, the firmware version was MA8_2_3.6)

B. TUNING AUTOPILOT PID GAINS

Chapter II mentioned that the Kestrel autopilot and Virtual Cockpit were developed by Procerus Technologies for the Zagi UAV test platforms. As the prototype KUAV is much smaller with different aerodynamic performance than the Zagi, there is a need to retune the PID gains of the autopilot to match the dynamic response of the prototype KUAV.

1. Aerodynamic Performance Parameters

The dimensionless coefficients from *LinAir* in Chapter V will again be used to define the aerodynamic performance of the prototype in the flight simulator, *Aviones*. The detailed procedures are presented in Appendix L.

2. Autopilot PID Gains

After setting up the model in *Aviones*, the PID gains of autopilot were tuned using the HIL simulation. The Ziegler Nichols rules were applied during tuning, with addition advice from Chapter II of the Kestrel Installation and Configuration Guide [16]. In addition, the author had also found the guidelines provided by Cloud Cap Technology [17] for tuning Piccolo autopilot to be useful during the process of tuning the gains on Kestrel autopilot. The final PID gains set on Kestrel autopilot are presented in Appendix M.

C. TEST SCENARIOS AND PROCEDURES

Given the short duration of this thesis and this being the first attempt to run HIL for Kestrel Autopilot the experiments were conducted with the following decisions in mind.

GPS waypoint navigation was used as the outer loop of the autopilot providing the guidance reference commands.

The PID gains were obtained using all available knowledge the author has on Virtual Cockpit and *Aviones*.

The aerodynamic performance parameters of the prototype were obtained from *LinAir*.

Therefore, the results might not be a true representation of the expected performance of the prototype KUAV but the processes will be beneficial for future works.

1. Test Scenarios and Procedures

A set of four waypoints (numbered 1 to 4) were set as the test route for the experiment. Waypoints 1 and 2 are set as intermediate positions for the UAV to reach the desired test altitude and speed. Waypoints 3 and 4 are on the actual test route, and waypoint 3 simulates the position where the KUAV is released from the HUAV. Waypoint 4 simulates the target position. Different release altitudes and horizontal ranges are achieved by adjusting the height and northing difference between waypoints 3 and 4 respectively.

A series of 7 runs, with velocities ranging from 6 m/s to 16 m/s at an interval of 2 m/s, were conducted. (This range of test velocities is selected based on the results obtained from both the analytical and 6DOF + AP models in the previous chapters.) The detailed procedures are presented in Appendix N.

D. RESULTS AND COMPARISON

Using the procedures described in Appendix N, six simulations were completed and the result of a sample case (velocity of 8 m/s) is presented below.

1. Results

Using the data generated from the HIL for a glide velocity of 8 m/s, the following graphs are plotted and shown in Figure 27.

The graph of H vs. R , provides insights to the L/D , glide angle and maximum horizontal range traveled by the KUAV during its descend from 300 m. (Typical operating ceiling for tactical systems.)

The graph of P vs. E , provides insights to the airborne endurance of the KUAV. It also shows the amount of transient the KUAU experiences after it is released from the HUAV. The average pitch angle will also be used to determine the AOA of the KUAV during its descend. The jump in pitch angle at the terminal phase is to be ignored as the KUAV had already landed on ground.

The graph of V vs. E , provides insights to the average velocity of the KUAV during its descend. It can also be observed from this graph that there is a transient period before steady-state condition is reached. The jump in velocity at the terminal phase is also to be ignored as the KUAV had already landed on ground.

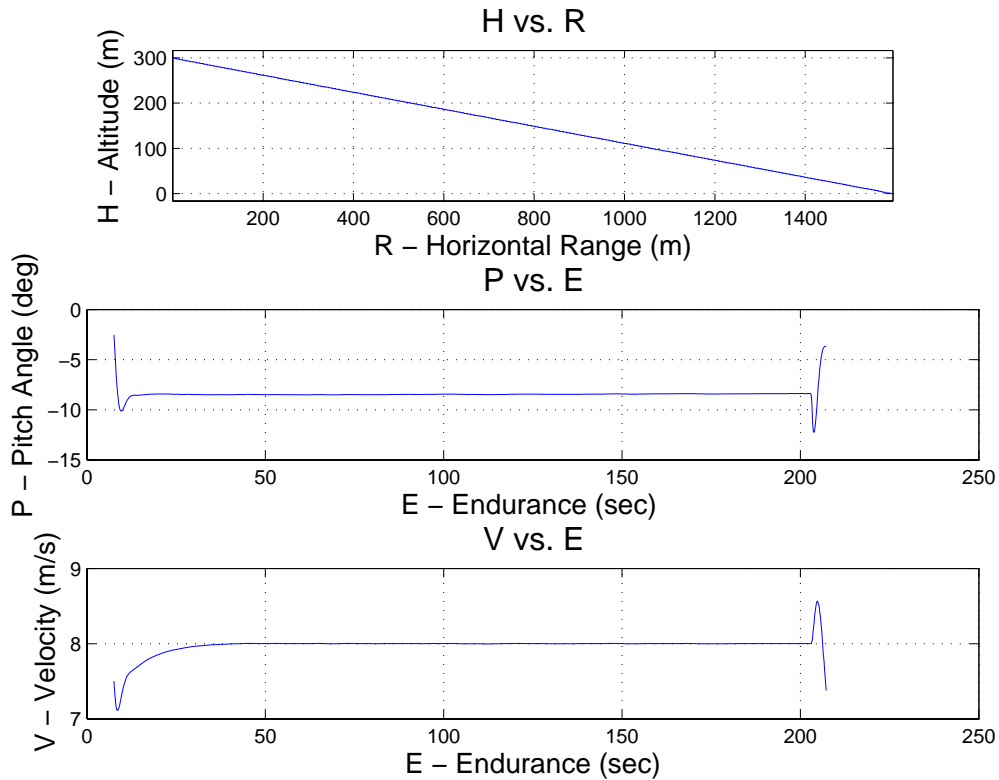


Figure 27. HIL results for a gliding velocity of 8m/s

The results for all the six simulations are summarized and attached in Appendix O.

2. Comparison

The results obtained from the HIL experiments were compared to those obtained from the analytical and the 6DOF + AP models. This comparison was only made for a small AOA range (until 4.5°) as this is the hardware's physical limits during actual implementation.

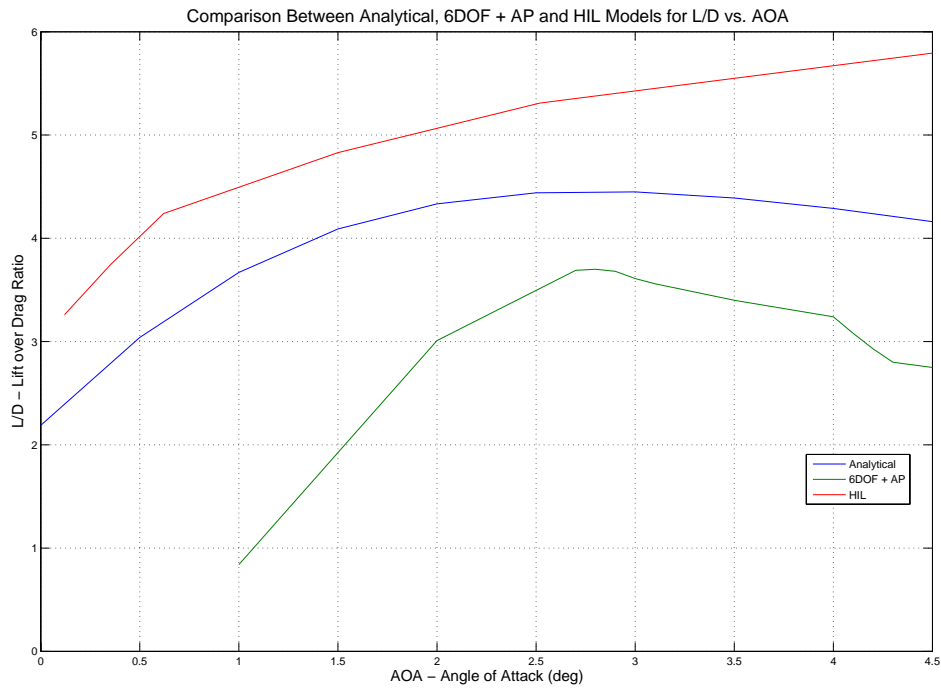


Figure 28. Comparison between analytical, 6DOF + AP and HIL models for L/D vs. AOA

Analysis of Figure 28 shows that the L/D computed from the HIL experiments displayed a similar trend but at a larger value as compared to those obtained in the analytical and 6DOF + AP models. In addition, the L/D value did not display a distinct point of maximum within this range of AOA . With the results from all 3 models displaying a similar trend, this further concludes the expected change of L/D with respect to changing AOA .

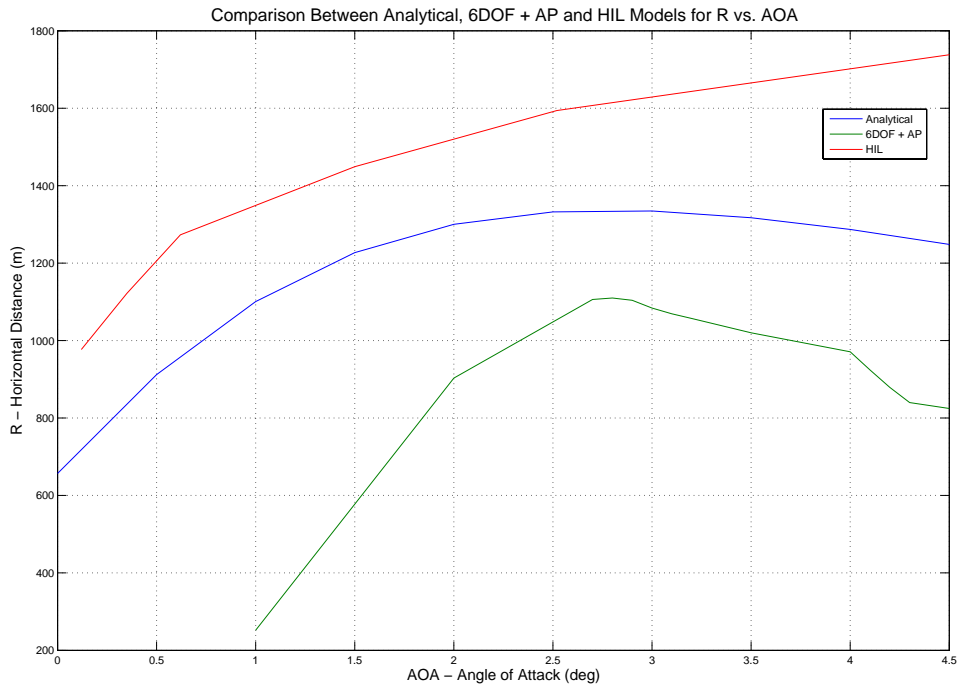


Figure 29. Comparison between analytical, 6DOF + AP and HIL models for R vs. AOA

Analysis of Figure 29 shows that the R computed from the HIL experiments displayed a similar trend but at a larger value as compared to those obtained in the analytical and 6DOF + AP models. This result is expected, as it is shown in Figure 27 that the values of L/D for HIL are larger. Similarly, the R value did not display a distinct point of maximum within this range of AOA . With the results from all 3 models displaying a similar trend, this further concludes the expected change of R with respect to changing AOA .

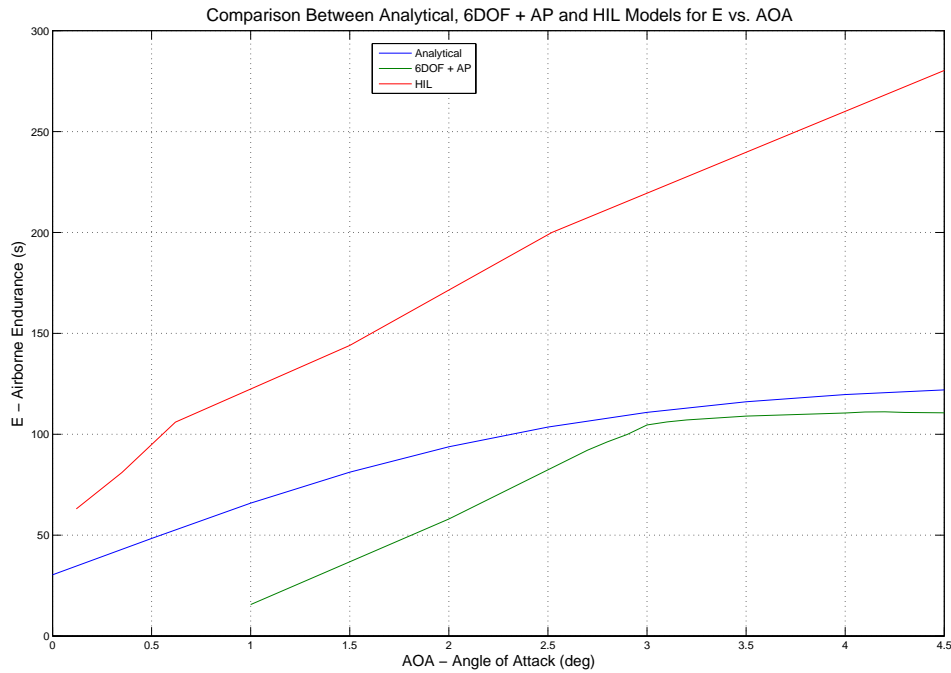


Figure 30. Comparison between analytical, 6DOF + AP and HIL models for E vs. AOA

Analysis of Figure 30 shows that the E computed from the HIL experiments displayed a similar trend as compared to those obtained in the analytical and 6DOF + AP models. However, at higher AOA where the velocity of the glider is lower, the E obtained from HIL is significantly larger. This is clearly different from the expected decrease in E with increasing AOA as predicted from the analytical and 6DOF + AP models.

The above results showed that the HIL model generates the same trend and behavior for E and R with changing AOA as compared to the analytical and the 6DOF + AP models. However, the results obtained from the HIL experiments were better than expected. Ideally, the results obtained from the HIL experiments should fall in between the upper and lower bound predicted by the analytical and the 6DOF + AP models respectively. This shows that the simulation model used by Kestrel is more optimistic than of the analytical model. There is a need for future studies to better understand the control and guidance architecture used in Kestrel autopilot. Apart from the uncertainty

caused by the autopilot, the aerodynamics parameters derived from *LinAir* might not be the actual representation of the KUAV's performance. The performance data will have to be refined after physical flight test. A detailed list of recommended future studies is presented in the next chapter.

VII. CONCLUSIONS

A. CONCLUSIONS

This thesis presented the concept of integrating COTS technologies to produce a prototype of a Tactical UCAV system. There is an existing HUAV developed and operated by the Naval Postgraduate School (NPS). For this reason, this thesis focused its effort on the design and evaluation of the performance of a non-powered glider with a wing that is linearly tapered and swept as the prototype KUAV.

As there was no readily available model in the market that could fulfill the requirements of the proposed KUAV, a prototype was physically built for experimentation. The prototype was made purely from COTS hobby-grade material and components. The prototype was trimmed for low-altitude, hand-launched RC flight.

The aerodynamic performances of the proposed prototype were first obtained using commercial panel code software. The aerodynamic performances were subsequently used in a Simulink 6DOF + AP software simulation, and the results obtained were comparable to those obtained from theoretical analysis.

HIL simulations were conducted using the default setting in Kestrel Autopilot. This was the first attempt to run HIL testing for the Kestrel Autopilot. One objective of running the HIL was to validate the performance of the prototype prior to a high-altitude autonomous AP test flight. The other main objective was to establish the correct system architecture and procedures for future studies.

Despite the short duration of this thesis, it shows that the proposed “Tactical UCAV” can be realized using COTS technologies. The following section describes some of the future studies required to reach the envisaged end product.

B. RECOMMENDATIONS AND FUTURE STUDIES

The following future studies are recommended for developing the proposed “Tactical UCAV” system:

1. Understanding the Kestrel Autopilot

There is a need to further understand the performance of the Kestrel autopilot. Given the short duration of this thesis, the current knowledge of the autopilot is superficial and insufficient to explain certain results or behaviors obtained from the HIL simulations.

2. Variations to Gliding Profile

This thesis had focused the research on investigating the maximum horizontal distance and airborne endurance the prototype can achieved given a released altitude. Future works should investigate the performance of the prototype for different glide profiles, for example the target is located right below the KUAV and not at a distance away.

3. Physical Integration with “Rascal”

“Rascal” is an SUAV developed and operated by the Naval Postgraduate School (NPS), and it will be the HUAV carrying the KUAV. There is a need to develop a mechanical device to carry and release the prototype from “Rascal”. Only with this device can the prototype be tested with high-altitude launches.

4. Data Integration with “Rascal”

Apart from developing the mechanical device to integrate the prototype with “Rascal,” there is also a need to establish an integrated method of communications for data transfers and updates between the HUAV and the KUAV. Two possible options are presented below for future works.

Option 1: Data transfers and updates are sent from the HUAV to the KUAV via Piccolo and Procerus ground stations as shown in Figure 31.

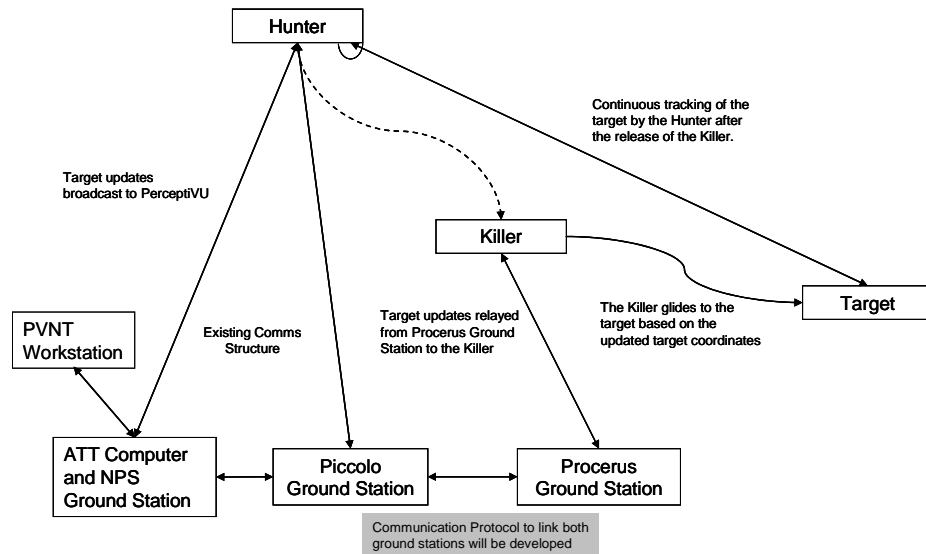


Figure 31. Communication protocol via ground control stations

Option 2: Data transfers and updates are sent directly from the HUAV to the KUAV via XBee (Radio Frequency Module developed by MaxStream, Inc.) as shown in Figure 32. This option is preferred as the prototype KUAV need not have connectivity with the Procerus ground station. Effectively, the Procerus ground station can be eliminated and target data are relayed to the prototype KUAV through the Hunter.

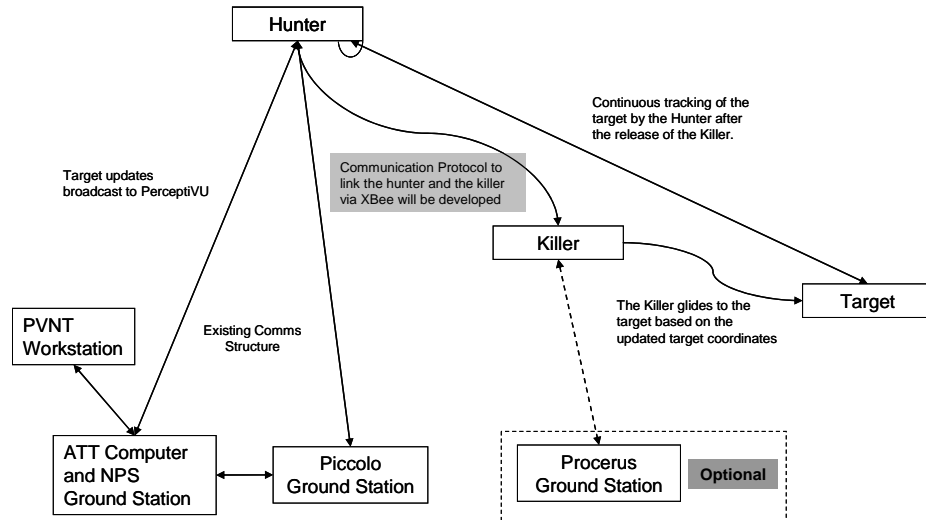


Figure 32. Communication protocol via radio frequency module

5. Variable Payload Capability for the KUAV

The current aerodynamic performances of the prototype were obtained based on a fixed payload. The effects of variable payloads should be investigated, as the proposed KUAV is capable of carry variable payloads.

APPENDIX A. TECHNICAL SPECIFICATIONS OF PREDATOR B



PREDATOR B

Persistent Multi-mission ISR and Strike Aircraft



OBJECTIVE
Perform multi-mission low- to high-altitude surveillance, reconnaissance, and “Hunter-Killer” missions.

CHARACTERISTICS	FEATURES
Wing Span: 66 ft (20m)	• Triple avionics
Length: 36 ft (11m)	• Redundant flight controls and control surfaces
Powerplant: Honeywell TPE 331-10T	• Remotely piloted or fully autonomous
Max Gross Takeoff Weight: 10,500 lb (4763 kg)	• Military Standard 1760 Stores Management System
Fuel Capacity: 4,000 lb (1814 kg)	• 6 wing stations for external carriage of payloads
Payload Capacity: 850 lb int. (385 kg)	• C-Band Line-of-Sight data link control
	• Ku-Band Beyond Line-of-Sight/SATCOM datalink control
Weapons: Hellfire missiles	• Over 90% system operational availability
GBU-12 laser-guided bombs	• Less than 12 hours displacement/emplacement
GBU-38 Joint Direct Attack Munitions	• C-130 transportable (or self deploys)
Power: 45 kVA, redundant	
Payloads: MTS-B EO/IR camera system	
Lynx SAR/GMTI	
Multi-mode maritime radar	
SIGINT/ESM system	
Communications relay	

PERFORMANCE

Max Altitude:	50,000+ ft
Max Endurance:	30+ hr
Max Air Speed:	240+ KTAS



THIS PAGE INTENTIONALLY LEFT BLANK

APPENDIX B. TECHNICAL SPECIFICATIONS OF SPERWER B

SPERWER B

SPERWER: the European reference in TUAV

Safe and airworthy design:

- Based on fail-safe and certified design
- Fully automated take-off and landing
- Advanced digital avionics suite
- Digital Ku band (15 GHz) data link
- Transponder/IFF mode 3C and VHF relay with ATC

Tactical capacity:

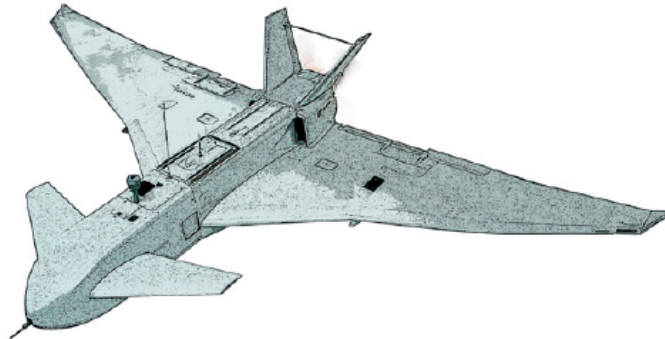
- High Mobility
- Operations from unprepared areas
- Day and Night operations
- C4I connection and Interoperability

Multi-payload capacity:

- EO/IR
- SAR
- Transmission relay
- EW (ELINT, COMINT)

Multi-mission capacity:

- ISTAR, targeting (20 m CEP)
- Long endurance (12+ hours)
- Weapon carrying capacity (60+ kg)
- Embedded sensor to shooter capability



100% SPERWER compatible:

- Ground Segment compatibility
 - same Catapult pneumatic launcher
 - same Ground Control Station and Ground Data Terminal
 - same Maintenance concept
 - same Training

- Other UAVs compatibility
 - dual UAV capability from single system
 - combined operation with: SPERWER STD, Fast Penetrator

Overall length:
3,5 m

Wing span:
6,8 m

Ceiling:
20,000 ft

Speed:
80 kts

Data link range:
200 km

Payload capacity:
100 kg

© - Photos: SAGMA, EBS - MPC/DF19 - 06/05

THIS PAGE INTENTIONALLY LEFT BLANK

APPENDIX C. TECHNICAL SPECIFICATIONS OF SHADOW 200

SHADOW 200: THE EYES OF THE COMMANDER



AAI is a world leader in the design, production, and sustainment of tactical unmanned aircraft systems in support of warfighters and peacekeeping missions.

Our Shadow 200s, known as the “eyes of the commander,” have exceeded 200,000 flight hours, more than 85 percent in support of Operation Iraqi Freedom. Shadow’s EO/IR payload sees targets 125 kilometers away from the brigade tactical operations center, providing situational awareness from an altitude up to 15,000 feet at more than 3.5 kilometers slant range, day or night.

Furthermore, our One System™ ground control station transmits imagery and telemetry data directly to Joint STARS, the All Sources Analysis Systems, and the Army Field Artillery Targeting and Direction System in near real time, delivering an unequalled interoperability network of intelligence-gathering capabilities.

As a quick deployment asset, Shadow 200 tactical unmanned aircraft systems can be flown anywhere in theater using C-130 aircraft.



U.S. Marines, who began transitioning to Shadow 200 systems in 2007, ready an aircraft for an intelligence-gathering sortie linked to a One System ground control station in the background.



Ground crew can prepare a launcher and ready a Shadow 200 aircraft for flight in a matter of minutes. The hydraulic launcher mounts on a standard high mobility trailer.

SYSTEM SPECIFICATIONS

Performance

- Endurance: 5-7 hours
- Max Altitude: 15,000 ft. (4,572 m)
- Max Dash Speed: 118 kts (218 kph)
- Cruise Speed: 90 kts (166 kph)
- Loiter Speed: 60 kts (110 kph)
- Takeoff Distance (Launcher): 30 ft. (10 m)

Features

- Advanced Composite Construction
- Combat-Proven Hardware
- Rotary Engine with Proven Performance
- Multiple Payload Capability
- Multiple Launch and Recovery Methods
- Operates with MOGAS
- Modular System Design for Deployment Flexibility

Technical Data

- Length: 11.2 ft. (3.41 m)
- Wingspan: 14 ft. (3.87 m)
- Max Payload: 45 - 60 lbs. (27 kg)
- Max Gross Weight: 375 lbs. (170 kg)

THIS PAGE INTENTIONALLY LEFT BLANK

APPENDIX D. TECHNICAL SPECIFICATIONS OF WATCHKEEPER TACTICAL UAV



SPECIFICATIONS - WATCHKEEPER TACTICAL UAV SYSTEM, UNITED KINGDOM

DIMENSIONS	
Wingspan (WK180)	6.00m
Wingspan (WK450)	10.51m
Length (WK180)	4.43m
Length (WK450)	6.10m
Fuselage Length (WK180)	3.47m
WEIGHTS	
Take-Off Weight (WK180)	195kg
Take-Off Weight (WK450)	450kg
Payload (WK180)	35kg
Payload (WK450)	150kg
PERFORMANCE	
Endurance (WK180)	More than 10 hours
Endurance (WK450)	20 or 30 hours
Altitude (WK180)	4,570m
Altitude (WK450)	5,480m
Loiter Speed (WK180)	130km/h
Loiter Speed (WK450)	100km/h
Maximum Speed (WK180)	194km/h
Maximum Speed (WK450)	175km/h
PROPULSION	
UEL AR 741 Engine (WK180)	28.3kW
UEL AR 801 Engine (WK450)	38.8kW

THIS PAGE INTENTIONALLY LEFT BLANK

APPENDIX E. COMPONENT SPECIFICATIONS

A. RC Mode

S/No	Items	Weight	Remarks
		grams	
RC Mode			
1	2 x Servo	10	
2	Radio Receiver	6	
3	Battery Pack	48.8	
4	Power Converter	6	
5	Nose Weight	6.9	Lead
Total		77.7	

Structural Weight **67.8** grams
Total Weight **145.5** grams

Effective Wing Area **71,438** mm²

Average Wing Loading **2.04E-03** grams/mm²

B. AP Mode

S/No	Items	Weight	Remarks
		grams	
AP Mode			
1	2 x Servo	10	
2	Auto Pilot	18	
3	Modem	13.8	
4	GPS Receiver	13.7	
5	Battery Pack	33.2	
6	Power Converter	6	
7	Cables	5	
8	Nose Weight	6.9	Lead
Total		106.6	

Structural Weight **67.8** grams
Total Weight **174.4** grams

Effective Wing Area **71,438** mm²

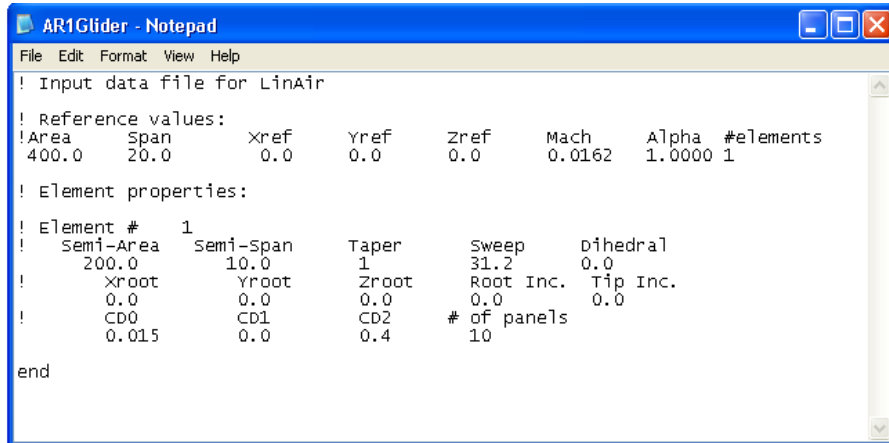
Average Wing Loading **2.44E-03** grams/mm²

THIS PAGE INTENTIONALLY LEFT BLANK

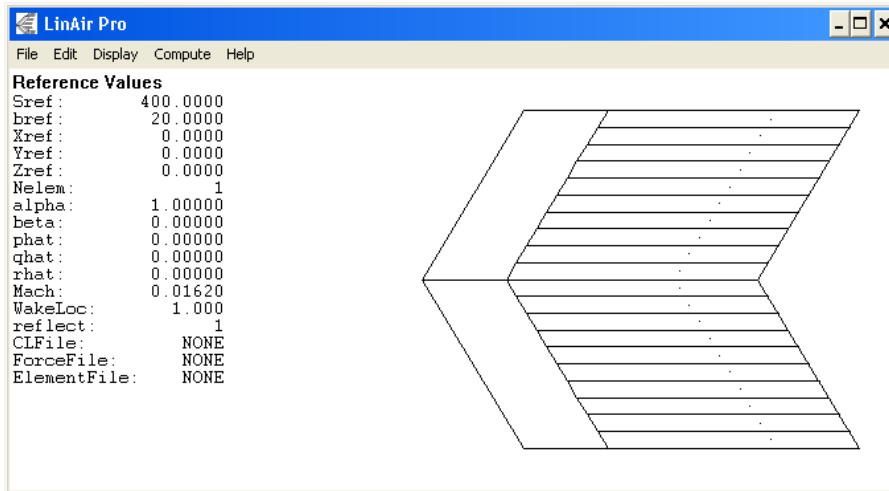
APPENDIX F. VERIFICATION OF PANEL CODES

A. $AR = 1$ at $Re = 70,000$

1. *LinAir* Input File ($CD0 = 0.015$ and $K = 0.4$)



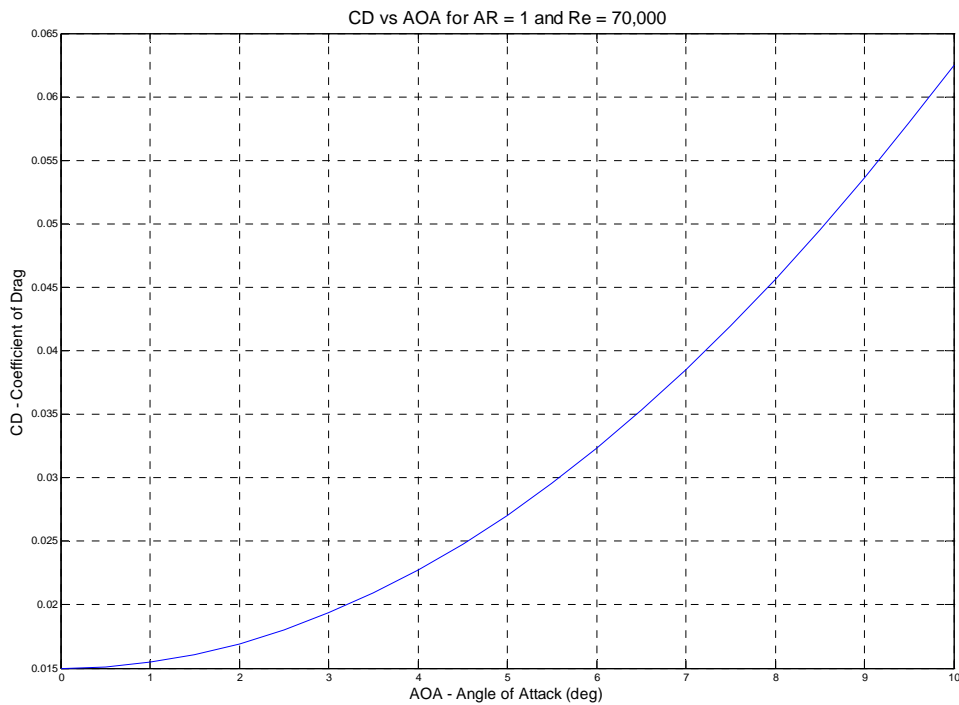
```
AR1Glider - Notepad
File Edit Format View Help
! Input data file for LinAir
! Reference values:
!Area   Span   xref   yref   zref   Mach   Alpha #elements
400.0   20.0    0.0    0.0    0.0    0.0162 1.0000 1
! Element properties:
! Element # 1
! Semi-Area Semi-Span Taper Sweep Dihedral
200.0     10.0     1     31.2    0.0
! Xroot Yroot Zroot Root Inc. Tip Inc.
0.0      0.0     0.0     0.0     0.0
! CD0 CD1 CD2 # of panels
0.015  0.0    0.4     10
end
```



2. Results generated by *LinAir*

AR1 - Notepad

File	Edit	Format	View	Help						
0.0	0.0	0.0	0.00000	0.01500	0.00000	0.00000	0.00000	0.00000	0.00000	0.00000
0.5	0.0	0.0	0.01290	0.01512	0.00000	-0.00174	0.00000	0.00000	0.00350	0.00000
1.0	0.0	0.0	0.02579	0.01548	0.00000	-0.00347	0.00000	0.00000	0.01368	0.00000
1.5	0.0	0.0	0.03867	0.01609	0.00000	-0.00520	0.00000	0.00000	0.02959	0.00000
2.0	0.0	0.0	0.05154	0.01694	0.00000	-0.00694	0.00000	0.00000	0.04993	0.00000
2.5	0.0	0.0	0.06438	0.01802	0.00000	-0.00867	0.00000	0.00000	0.07320	0.00000
3.0	0.0	0.0	0.07720	0.01935	0.00000	-0.01041	0.00000	0.00000	0.09802	0.00000
3.5	0.0	0.0	0.08998	0.02092	0.00000	-0.01214	0.00000	0.00000	0.12319	0.00000
4.0	0.0	0.0	0.10272	0.02273	0.00000	-0.01387	0.00000	0.00000	0.14779	0.00000
4.5	0.0	0.0	0.11542	0.02477	0.00000	-0.01560	0.00000	0.00000	0.17118	0.00000
5.0	0.0	0.0	0.12806	0.02705	0.00000	-0.01733	0.00000	0.00000	0.19298	0.00000
5.5	0.0	0.0	0.14065	0.02957	0.00000	-0.01905	0.00000	0.00000	0.21298	0.00000
6.0	0.0	0.0	0.15318	0.03232	0.00000	-0.02078	0.00000	0.00000	0.23112	0.00000
6.5	0.0	0.0	0.16565	0.03530	0.00000	-0.02250	0.00000	0.00000	0.24743	0.00000
7.0	0.0	0.0	0.17804	0.03851	0.00000	-0.02423	0.00000	0.00000	0.26199	0.00000
7.5	0.0	0.0	0.19035	0.04195	0.00000	-0.02595	0.00000	0.00000	0.27492	0.00000
8.0	0.0	0.0	0.20258	0.04562	0.00000	-0.02766	0.00000	0.00000	0.28635	0.00000
8.5	0.0	0.0	0.21473	0.04951	0.00000	-0.02938	0.00000	0.00000	0.29643	0.00000
9.0	0.0	0.0	0.22678	0.05363	0.00000	-0.03109	0.00000	0.00000	0.30527	0.00000
9.5	0.0	0.0	0.23873	0.05796	0.00000	-0.03280	0.00000	0.00000	0.31300	0.00000
10.0	0.0	0.0	0.25059	0.06251	0.00000	-0.03451	0.00000	0.00000	0.31974	0.00000

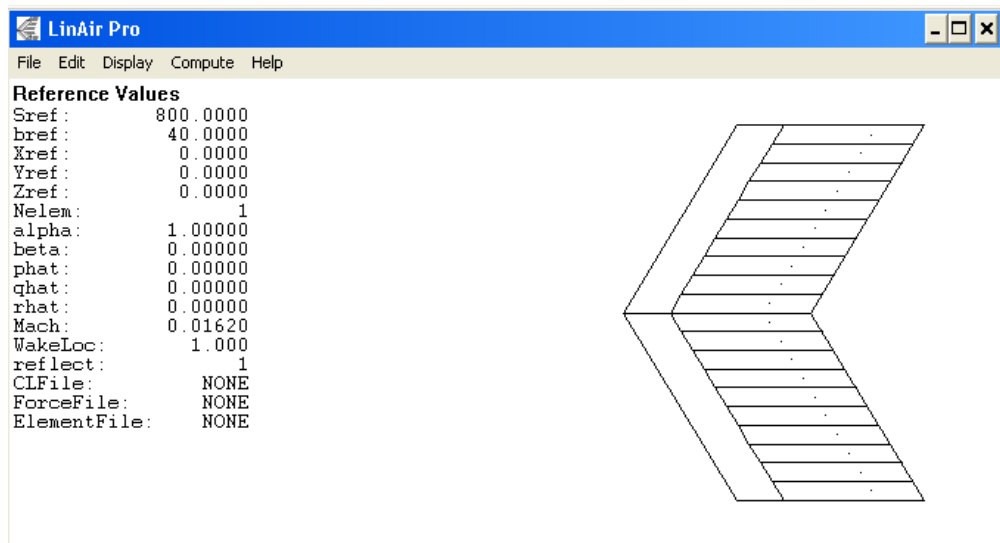


The above results, generated by *LinAir* for the AOA range of 0° to 10° , closely matched the results obtained in the wind tunnel experiments conducted by [12].

B. $AR = 2$ at $Re = 70,000$

1. *LinAir* Input File ($CD0 = 0.020$ and $K = 0.4$)

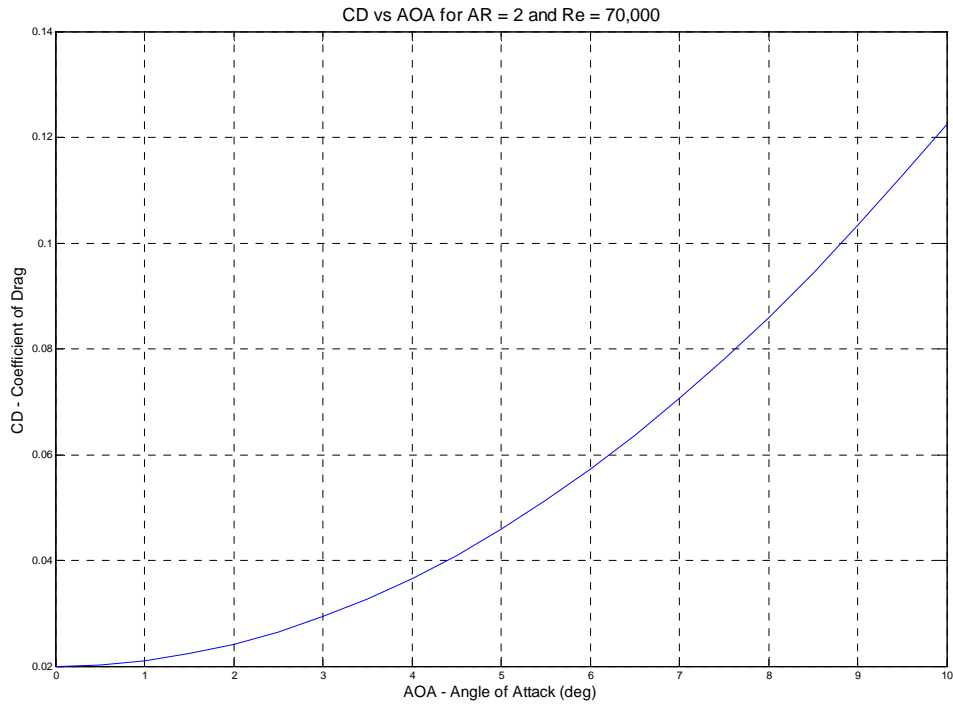
```
AR2Glider - Notepad
File Edit Format View Help
! Input data file for LinAir
! Reference values:
!Area   Span   xref    yref    zref    Mach   Alpha  #elements
800.0   40.0    0.0     0.0     0.0     0.0162 1.0    1
! Element properties:
! Element # 1
! Semi-Area Semi-Span Taper Sweep dihedral
400.0      20.0     1      31.2    0
! Xroot Yroot Zroot Root Inc. Tip Inc.
0.0      0.0     0.0     0.0     0
! CD0 CD1 CD2 # of panels
0.020    0      0.4     10
end
```



2. Results generated by *LinAir*

AR2 - Notepad

File	Edit	Format	View	Help						
0.0	0.0	0.0	0.00000	0.02000	0.00000	0.00000	0.00000	0.00000	0.00000	0.00000
0.5	0.0	0.0	0.02139	0.02026	0.00000	-0.00580	0.00000	0.00000	0.00361	
1.0	0.0	0.0	0.04278	0.02104	0.00000	-0.01161	0.00000	0.00000	0.01389	
1.5	0.0	0.0	0.06415	0.02234	0.00000	-0.01741	0.00000	0.00000	0.02941	
2.0	0.0	0.0	0.08548	0.02416	0.00000	-0.02322	0.00000	0.00000	0.04830	
2.5	0.0	0.0	0.10678	0.02650	0.00000	-0.02903	0.00000	0.00000	0.06872	
3.0	0.0	0.0	0.12804	0.02935	0.00000	-0.03484	0.00000	0.00000	0.08918	
3.5	0.0	0.0	0.14923	0.03272	0.00000	-0.04065	0.00000	0.00000	0.10868	
4.0	0.0	0.0	0.17036	0.03661	0.00000	-0.04647	0.00000	0.00000	0.12659	
4.5	0.0	0.0	0.19141	0.04101	0.00000	-0.05229	0.00000	0.00000	0.14268	
5.0	0.0	0.0	0.21238	0.04592	0.00000	-0.05811	0.00000	0.00000	0.15687	
5.5	0.0	0.0	0.23325	0.05133	0.00000	-0.06393	0.00000	0.00000	0.16924	
6.0	0.0	0.0	0.25402	0.05726	0.00000	-0.06976	0.00000	0.00000	0.17996	
6.5	0.0	0.0	0.27468	0.06369	0.00000	-0.07560	0.00000	0.00000	0.18918	
7.0	0.0	0.0	0.29522	0.07062	0.00000	-0.08144	0.00000	0.00000	0.19708	
7.5	0.0	0.0	0.31562	0.07804	0.00000	-0.08729	0.00000	0.00000	0.20382	
8.0	0.0	0.0	0.33589	0.08597	0.00000	-0.09314	0.00000	0.00000	0.20957	
8.5	0.0	0.0	0.35601	0.09438	0.00000	-0.09899	0.00000	0.00000	0.21444	
9.0	0.0	0.0	0.37597	0.10328	0.00000	-0.10486	0.00000	0.00000	0.21855	
9.5	0.0	0.0	0.39577	0.11267	0.00000	-0.11073	0.00000	0.00000	0.22199	
10.0	0.0	0.0	0.41539	0.12253	0.00000	-0.11661	0.00000	0.00000	0.22486	



The above results, generated by *LinAir* for the AOA range of 0° to 10° , closely matched the results obtained in the wind tunnel experiments conducted by [12].

APPENDIX G. INPUT FILE FOR PANEL CODE

```

Binch_Glider - Notepad
File Edit Format View Help
! Input data file for LinAir

! Reference values:
!Area   Span   Xref  Yref  Zref  Mach   Alpha  #elements
90516.0 501.8   0.0   0.0   0.0   0.0179 1.0    2

! Element properties:

! Element #    1
! Semi-Area   Semi-Span   Taper      Sweep      Dihedral
35719.0     250.9       0.776      34.3       0.0
! Xroot       Yroot       Zroot      Root Inc.  Tip Inc.
0.0         0.0         0.0        0.0        0.0
! CD0         CD1         CD2        # of panels
0.022      0.0         0.4        10

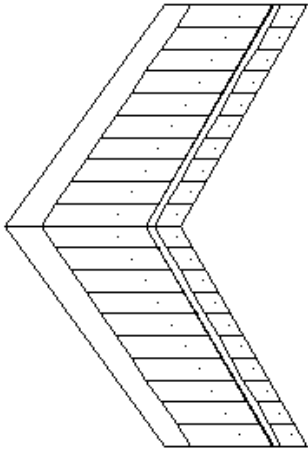
! Element #    2
! Semi-Area   Semi-Span   Taper      Sweep      Dihedral
9539.0      250.9       1.0        29.9       0.0
! Xroot       Yroot       Zroot      Root Inc.  Tip Inc.
129.5       0.0         0.0        0.0        0.0
! CD0         CD1         CD2        # of panels
0.022      0.0         0.4        10

end
    
```

```

LinAir Pro
File Edit Display Compute Help

Reference Values
Sref:    90516.0000
bref:    501.8000
Xref:    0.0000
Yref:    0.0000
Zref:    0.0000
Nelem:   2
alpha:   1.00000
beta:    0.00000
phat:    0.00000
qhat:    0.00000
rhat:    0.00000
Mach:    0.01790
WakeLoc: 1.000
reflect: 1
CLFile:  NONE
ForceFile: NONE
ElementFile: NONE
    
```



THIS PAGE INTENTIONALLY LEFT BLANK

APPENDIX H. DATA FILE GENERATED BY PANEL CODE

Results for non-cambered airfoil

The image shows a Notepad window titled "Binf1 - Notepad" containing a data file. The data is organized into 10 columns and 41 rows. The first three columns contain the values 0.0, 0.0, and 0.0 for every row. The remaining seven columns contain numerical values that vary across the rows, representing aerodynamic data for a non-cambered airfoil. The values in the 4th, 5th, and 6th columns are positive, while the values in the 7th, 8th, and 9th columns are negative. The 10th column contains positive values that generally increase from top to bottom.

0.0	0.0	0.0	0.00000	0.02200	0.00000	0.00000	0.00000	0.00000	0.00000
0.5	0.0	0.0	0.02574	0.02238	0.00000	-0.01231	0.00000	0.00000	0.00339
1.0	0.0	0.0	0.05147	0.02351	0.00000	-0.02463	0.00000	0.00000	0.01289
1.5	0.0	0.0	0.07718	0.02539	0.00000	-0.03695	0.00000	0.00000	0.02684
2.0	0.0	0.0	0.10285	0.02803	0.00000	-0.04928	0.00000	0.00000	0.04319
2.5	0.0	0.0	0.12848	0.03141	0.00000	-0.06161	0.00000	0.00000	0.06013
3.0	0.0	0.0	0.15406	0.03555	0.00000	-0.07396	0.00000	0.00000	0.07639
3.5	0.0	0.0	0.17958	0.04044	0.00000	-0.08632	0.00000	0.00000	0.09124
4.0	0.0	0.0	0.20501	0.04608	0.00000	-0.09870	0.00000	0.00000	0.10437
4.5	0.0	0.0	0.23037	0.05247	0.00000	-0.11109	0.00000	0.00000	0.11574
5.0	0.0	0.0	0.25562	0.05959	0.00000	-0.12350	0.00000	0.00000	0.12546
5.5	0.0	0.0	0.28077	0.06747	0.00000	-0.13594	0.00000	0.00000	0.13370
6.0	0.0	0.0	0.30580	0.07608	0.00000	-0.14840	0.00000	0.00000	0.14064
6.5	0.0	0.0	0.33071	0.08543	0.00000	-0.16089	0.00000	0.00000	0.14648
7.0	0.0	0.0	0.35547	0.09552	0.00000	-0.17340	0.00000	0.00000	0.15136
7.5	0.0	0.0	0.38009	0.10635	0.00000	-0.18595	0.00000	0.00000	0.15544
8.0	0.0	0.0	0.40455	0.11790	0.00000	-0.19854	0.00000	0.00000	0.15884
8.5	0.0	0.0	0.42884	0.13018	0.00000	-0.21115	0.00000	0.00000	0.16165
9.0	0.0	0.0	0.45295	0.14318	0.00000	-0.22381	0.00000	0.00000	0.16396
9.5	0.0	0.0	0.47688	0.15690	0.00000	-0.23651	0.00000	0.00000	0.16584
10.0	0.0	0.0	0.50061	0.17134	0.00000	-0.24925	0.00000	0.00000	0.16735
10.5	0.0	0.0	0.52413	0.18650	0.00000	-0.26203	0.00000	0.00000	0.16855
11.0	0.0	0.0	0.54743	0.20236	0.00000	-0.27487	0.00000	0.00000	0.16946
11.5	0.0	0.0	0.57051	0.21892	0.00000	-0.28775	0.00000	0.00000	0.17012
12.0	0.0	0.0	0.59335	0.23618	0.00000	-0.30069	0.00000	0.00000	0.17057
12.5	0.0	0.0	0.61596	0.25414	0.00000	-0.31368	0.00000	0.00000	0.17082
13.0	0.0	0.0	0.63830	0.27278	0.00000	-0.32673	0.00000	0.00000	0.17090
13.5	0.0	0.0	0.66039	0.29211	0.00000	-0.33983	0.00000	0.00000	0.17083
14.0	0.0	0.0	0.68221	0.31212	0.00000	-0.35300	0.00000	0.00000	0.17062
14.5	0.0	0.0	0.70375	0.33280	0.00000	-0.36623	0.00000	0.00000	0.17028
15.0	0.0	0.0	0.72500	0.35414	0.00000	-0.37953	0.00000	0.00000	0.16983
15.5	0.0	0.0	0.74596	0.37615	0.00000	-0.39290	0.00000	0.00000	0.16927
16.0	0.0	0.0	0.76662	0.39881	0.00000	-0.40634	0.00000	0.00000	0.16862
16.5	0.0	0.0	0.78696	0.42212	0.00000	-0.41985	0.00000	0.00000	0.16788
17.0	0.0	0.0	0.80700	0.44607	0.00000	-0.43344	0.00000	0.00000	0.16705
17.5	0.0	0.0	0.82670	0.47065	0.00000	-0.44710	0.00000	0.00000	0.16616
18.0	0.0	0.0	0.84608	0.49586	0.00000	-0.46085	0.00000	0.00000	0.16519
18.5	0.0	0.0	0.86512	0.52169	0.00000	-0.47468	0.00000	0.00000	0.16416
19.0	0.0	0.0	0.88382	0.54814	0.00000	-0.48859	0.00000	0.00000	0.16306
19.5	0.0	0.0	0.90217	0.57518	0.00000	-0.50259	0.00000	0.00000	0.16191
20.0	0.0	0.0	0.92016	0.60283	0.00000	-0.51668	0.00000	0.00000	0.16071
20.5	0.0	0.0	0.93778	0.63106	0.00000	-0.53086	0.00000	0.00000	0.15946
21.0	0.0	0.0	0.95505	0.65987	0.00000	-0.54513	0.00000	0.00000	0.15816

Results for cambered airfoil

Angle of Attack	Angle of Sideslip	Free Stream Mach Number	Lift Coefficient	Drag Coefficient	Sideforce Coefficient	Moment Coefficient	Rolling Moment Coefficient	Yawing Moment Coefficient	Span Efficiency
0.0	0.0	0.0	0.05147	0.02351	0.00000	-0.02463	0.00000	0.00000	0.01289
0.5	0.0	0.0	0.07718	0.02539	0.00000	-0.03695	0.00000	0.00000	0.02684
1.0	0.0	0.0	0.10285	0.02803	0.00000	-0.04928	0.00000	0.00000	0.04319
1.5	0.0	0.0	0.12848	0.03141	0.00000	-0.06161	0.00000	0.00000	0.06013
2.0	0.0	0.0	0.15406	0.03555	0.00000	-0.07396	0.00000	0.00000	0.07639
2.5	0.0	0.0	0.17958	0.04044	0.00000	-0.08632	0.00000	0.00000	0.09124
3.0	0.0	0.0	0.20501	0.04608	0.00000	-0.09870	0.00000	0.00000	0.10437
3.5	0.0	0.0	0.23037	0.05247	0.00000	-0.11109	0.00000	0.00000	0.11574
4.0	0.0	0.0	0.25562	0.05959	0.00000	-0.12350	0.00000	0.00000	0.12546
4.5	0.0	0.0	0.28077	0.06747	0.00000	-0.13594	0.00000	0.00000	0.13370
5.0	0.0	0.0	0.30580	0.07608	0.00000	-0.14840	0.00000	0.00000	0.14064
5.5	0.0	0.0	0.33071	0.08543	0.00000	-0.16089	0.00000	0.00000	0.14648
6.0	0.0	0.0	0.35547	0.09552	0.00000	-0.17340	0.00000	0.00000	0.15136
6.5	0.0	0.0	0.38009	0.10635	0.00000	-0.18595	0.00000	0.00000	0.15544
7.0	0.0	0.0	0.40455	0.11790	0.00000	-0.19854	0.00000	0.00000	0.15884
7.5	0.0	0.0	0.42884	0.13018	0.00000	-0.21115	0.00000	0.00000	0.16165
8.0	0.0	0.0	0.45295	0.14318	0.00000	-0.22381	0.00000	0.00000	0.16396
8.5	0.0	0.0	0.47688	0.15690	0.00000	-0.23651	0.00000	0.00000	0.16584
9.0	0.0	0.0	0.50061	0.17134	0.00000	-0.24925	0.00000	0.00000	0.16735
9.5	0.0	0.0	0.52413	0.18650	0.00000	-0.26203	0.00000	0.00000	0.16855
10.0	0.0	0.0	0.54743	0.20236	0.00000	-0.27487	0.00000	0.00000	0.16946
10.5	0.0	0.0	0.57051	0.21892	0.00000	-0.28775	0.00000	0.00000	0.17012
11.0	0.0	0.0	0.59335	0.23618	0.00000	-0.30069	0.00000	0.00000	0.17057
11.5	0.0	0.0	0.61596	0.25414	0.00000	-0.31368	0.00000	0.00000	0.17082
12.0	0.0	0.0	0.63830	0.27278	0.00000	-0.32673	0.00000	0.00000	0.17090
12.5	0.0	0.0	0.66039	0.29211	0.00000	-0.33983	0.00000	0.00000	0.17083
13.0	0.0	0.0	0.68221	0.31212	0.00000	-0.35300	0.00000	0.00000	0.17062
13.5	0.0	0.0	0.70375	0.33280	0.00000	-0.36623	0.00000	0.00000	0.17028
14.0	0.0	0.0	0.72500	0.35414	0.00000	-0.37953	0.00000	0.00000	0.16983
14.5	0.0	0.0	0.74596	0.37615	0.00000	-0.39290	0.00000	0.00000	0.16927
15.0	0.0	0.0	0.76662	0.39881	0.00000	-0.40634	0.00000	0.00000	0.16862
15.5	0.0	0.0	0.78696	0.42212	0.00000	-0.41985	0.00000	0.00000	0.16788
16.0	0.0	0.0	0.80700	0.44607	0.00000	-0.43344	0.00000	0.00000	0.16705
16.5	0.0	0.0	0.82670	0.47065	0.00000	-0.44710	0.00000	0.00000	0.16616
17.0	0.0	0.0	0.84608	0.49586	0.00000	-0.46085	0.00000	0.00000	0.16519
17.5	0.0	0.0	0.86512	0.52169	0.00000	-0.47468	0.00000	0.00000	0.16416
18.0	0.0	0.0	0.88382	0.54814	0.00000	-0.48859	0.00000	0.00000	0.16306
18.5	0.0	0.0	0.90217	0.57518	0.00000	-0.50259	0.00000	0.00000	0.16191
19.0	0.0	0.0	0.92016	0.60283	0.00000	-0.51668	0.00000	0.00000	0.16071
19.5	0.0	0.0	0.93778	0.63106	0.00000	-0.53086	0.00000	0.00000	0.15946
20.0	0.0	0.0	0.95505	0.65987	0.00000	-0.54513	0.00000	0.00000	0.15816

- Column 1 = Angle of Attack
- Column 2 = Angle of Sideslip
- Column 3 = Free Stream Mach Number
- Column 4 = Lift Coefficient
- Column 5 = Drag Coefficient
- Column 6 = Sideforce Coefficient
- Column 7 = Moment Coefficient
- Column 8 = Rolling Moment Coefficient
- Column 9 = Yawing Moment Coefficient
- Column 10 = Span Efficiency

APPENDIX I. INITIALIZATION FILE FOR 6DOF + AP MODEL

```
% Initialization file for 6DOF + AP simulation model.

clc;
T=0.1;
r_lim=7;
% Initial Conditions in ENU (all vector data is represented as a column
vectors)
Pos_0   = [0; 0; 300]';           % Initial position vector (m)
Euler_0 = [0; 0; 0]'*pi/180;     % Initial Euler angles (rad)
Omega_0 = [0; 0; 0]';           % Initial Omega (rad/s)
PQR_0   = [0; 0; 0]';           % Initial Omega (rad/s)
Vb_0    = [5; 0; 0]';           % Initial body-velocity vector (m/s)

% Mass and Geometric Parameters recomputation
S       = (0.2032+0.1576)*0.5018/2; % Surface area of wing (m2)
span    = 0.5018;                 % wingspan (m)
chord   = 0.1814;                 % Mean Aerodynamic Chord (m)
mass    = 0.175;                  % gross weight (kg)
Ixx     = 0.0028959;              % main moment of inertia around axis Ox (kg*sq.m)
Iyy     = 0.0006514;              % main moment of inertia around axis Oy (kg*sq.m)
Izz     = 0.0035430;              % main moment of inertia around axis Oz (kg*sq.m)

% Aerodynamic Derivatives (all per radian)
CL0     = 0.05147; % lift coefficient at a = 0
CLa     = 2.9095; % lift curve slope
CLa_dot = 0;      % lift due to angle of attack rate
CLq     = 0;      % lift due to pitch rate
CLDe    = -1.3776; % lift due to elevator
CD0     = 0.0220; % drag coefficient at a = 0
Apolars = 0.5229; % drag curve slope (A2) CD=CD0+A2*1.25*CL^2
A1      = 0;
CYb     = 0;      % side force due to sideslip
CYDr    = 0;      % sideforce due to rudder
Clb     = -0.00172; % dihedral effect = -0.00172
Clp     = 0;      % roll damping
Clr     = 0;      % roll due to yaw rate
ClDa    = 0;      % roll control power
ClDr    = 0;      % roll due to rudder
Cm0     = -0.02463; % pitch moment at a = 0
Cma     = -1.4192; % pitch moment due to angle of attack
Cma_dot = 0;      % pitch moment due to angle of attack rate
Cmq     = 0;      % pitch moment due to pitch rate
CmDe    = -1.1543; % pitch control power
Cnb     = 0;      % weathercock stability
Cnp     = 0;      % adverse yaw
Cnr     = 0;      % yaw damping
CnDa    = 0;      % aileron adverse yaw
CnDr    = 0;      % yaw control power
CLDf    = -1.3776; % lift due to flap
CmDf    = -1.1543; % flap control power
```

```
% Standard Atmosphere
ISA_lapse = .0065;           % Lapse rate           (degC/m)
ISA_hmax  = 2000;           % Altitude limit      (m)
ISA_R     = 287;            % Gas Constant         (degK*m*m/s/s)
ISA_g     = 9.815;          % Gravity              (m/s/s)
ISA_rho0  = 1.225;          % Density at sea level (kg/m/m/m)
ISA_P0    = 101325;         % Sea-level Pressure   (N/m/m)
ISA_T0    = 289;            % Sea-level Temperature (degK)
```

APPENDIX J. SIMULATION RESULTS FROM THE 6DOF + AP MODEL

AOA (deg)	E (s)	R (m)	V (m/s)	L/D
1.0	15.6	252	32.7	0.84
2.0	58.0	903	16.1	3.01
2.7	92.1	1106	12.5	3.69
2.8	96.2	1110	12.0	3.70
2.9	99.9	1104	11.5	3.68
3.0	104.6	1084	10.7	3.61
3.1	106.1	1069	10.5	3.56
3.2	107.1	1057	10.3	3.52
3.5	109.0	1020	9.8	3.40
4.0	110.5	971	9.2	3.24
4.1	111.0	924	8.8	3.08
4.2	111.1	879	8.4	2.93
4.3	110.8	840	8.0	2.80
5.0	110.2	786	7.6	2.62
6.0	107.3	624	6.5	2.08
7.0	105.5	516	5.7	1.72
8.0	105.0	461	5.3	1.54

THIS PAGE INTENTIONALLY LEFT BLANK

APPENDIX K. PROCEDURES FOR SETTING UP THE TCP/IP CONNECTION

The following set of procedures is used to set up the TCP/IP connection for the HIL experiments.

Remove the modem from the autopilot.

Disconnect the programming wire on the programming cable as shown in Figure 33.

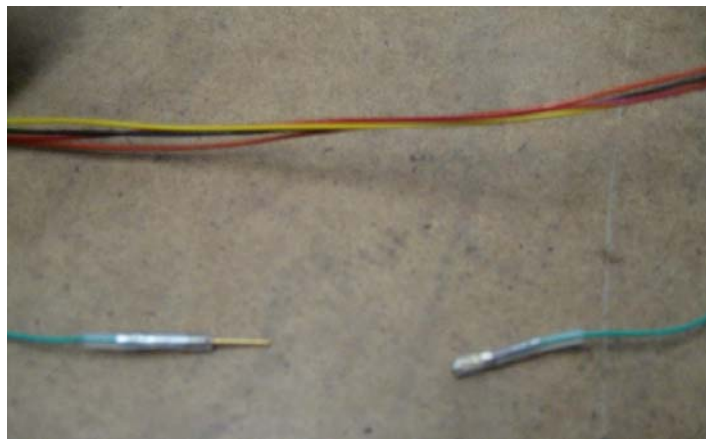


Figure 33. Disconnected programming wire

Plug the 5 pin header of the programming cable into the autopilot modem port as shown in Figure 34. The top cable is the programming cable, and the bottom cable is the power cable.



Figure 34. Connection for the programming and power cables on autopilot

Plug the other end of the programming cable into a free serial port on the computer that will be running Virtual Cockpit.

Power on the autopilot.

Load Aviones.

Load Virtual Cockpit.

Open the “**Edit Agents**” window in Virtual Cockpit. (This can be found in the “**Agent Menu**”) The right-most column is labeled “**HIL**” for hardware-in-the-loop. Check the box next to the agent number of the autopilot as shown in Figure 35.

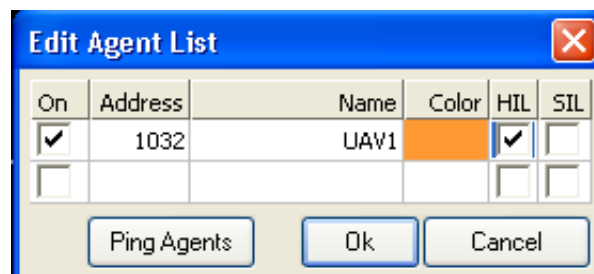


Figure 35. HIL selection in Virtual Cockpit

Click “**OK**.”

A dialog box will pop up (see Figure 36) in which the IP address of the computer running Aviones may be specified. If Aviones is running on the same computer that is running Virtual Cockpit, click the “**Loopback**” button and click “**OK**” to connect to Aviones. Virtual Cockpit will now attempt to connect to Aviones and add all the selected agents that had the HIL checkboxes checked.

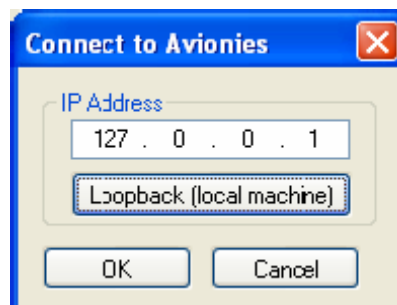


Figure 36. Connection window for Aviones

If connected successfully, the Virtual Cockpit will indicate on its status bar and Aviones will have added the Agent to its list on the bottom of the window, as shown in Figure 37.

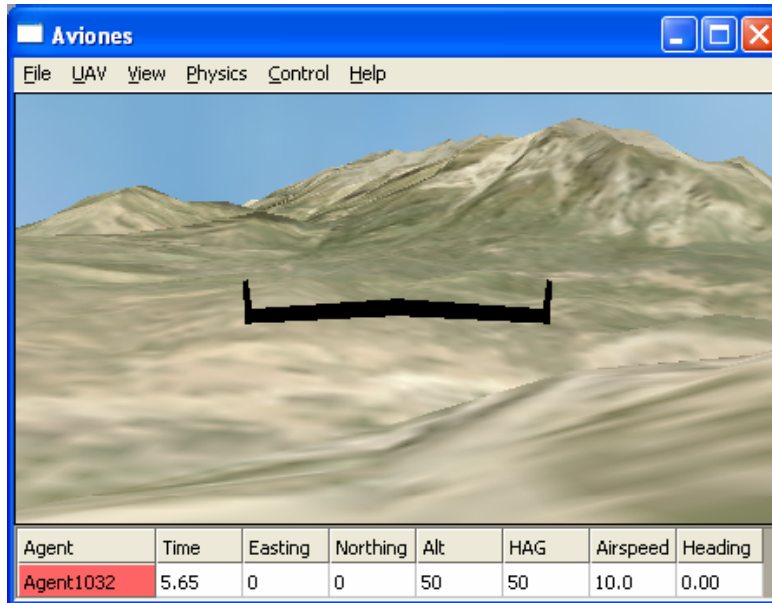


Figure 37. Agent added in Aviones

The next step is to make sure that Aviones is set up to talk to the autopilot through the correct comm port. Open up the HIL simulation control dialog in Aviones through “**View Menu**” followed by “**HIL Sim Ctrl**”.

Place the cursor in the Serial Port # box.

Delete the value that is currently in the box using the backspace key. (The box should turn red)

Enter the serial port number connected to the autopilot.

Click “**Enter**” – The box should turn white and the word “Open” should be displayed in the box to the right as shown in Figure 38.

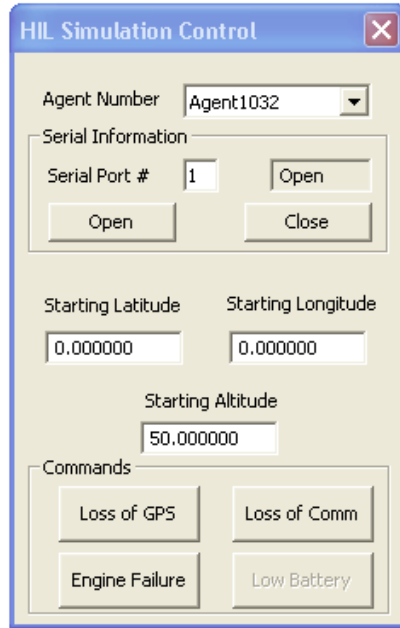


Figure 38. HIL simulation control window

With the correct serial port open, data should begin to flow between Aviones, Virtual Cockpit and the autopilot. Virtual Cockpit should show communications with the autopilot.

To verify communication between Aviones and the autopilot, the right-most LED on the autopilot should be blinking rapidly. This indicates that the autopilot is receiving sensor information from Aviones.

The final display on the user interfaces for Aviones and Virtual Cockpit (if there is a successful connection) is shown in Figure 39.

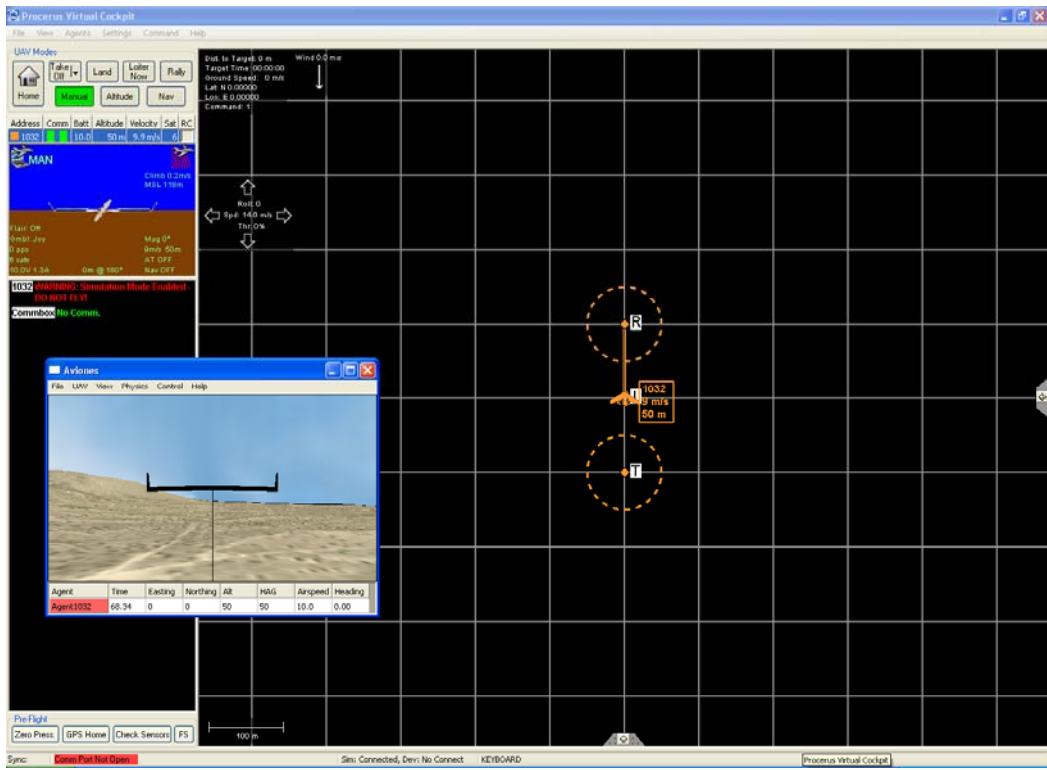


Figure 39. User interfaces for Avionics and Virtual Cockpit

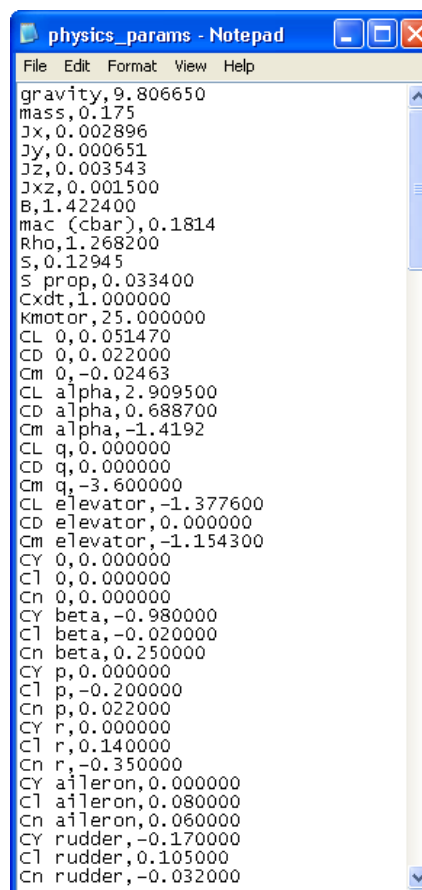
THIS PAGE INTENTIONALLY LEFT BLANK

APPENDIX L. PROCEDURES FOR UPDATING AERODYNAMIC PERFORMANCE PARAMETERS IN AVIONES

The initial performance parameters loaded in Aviones were for Zagi UAV test platform. The procedures for updating these performance parameters are as follows.

Locate the initialization text file, “physics_params” in the Aviones folder.

Change the necessary parameters to match the performance of the prototype. The updated parameters for this thesis are shown in Figure 40.



```
physics_params - Notepad
File Edit Format View Help
gravity,9.806650
mass,0.175
Jx,0.002896
Jy,0.000651
Jz,0.003543
Jxz,0.001500
B,1.422400
mac (cbar),0.1814
rho,1.268200
S,0.12945
S prop,0.033400
Cxdt,1.000000
Kmotor,25.000000
CL 0,0.051470
CD 0,0.022000
Cm 0,-0.02463
CL alpha,2.909500
CD alpha,0.688700
Cm alpha,-1.4192
CL q,0.000000
CD q,0.000000
Cm q,-3.600000
CL elevator,-1.377600
CD elevator,0.000000
Cm elevator,-1.154300
CY 0,0.000000
CL 0,0.000000
Cn 0,0.000000
CY beta,-0.980000
CL beta,-0.020000
Cn beta,0.250000
CY p,0.000000
CL p,-0.200000
Cn p,0.022000
CY r,0.000000
CL r,0.140000
Cn r,-0.350000
CY aileron,0.000000
CL aileron,0.080000
Cn aileron,0.060000
CY rudder,-0.170000
CL rudder,0.105000
Cn rudder,-0.032000
```

Figure 40. Aerodynamic performance coefficients for prototype

Save the changes. (Do not change the file name)

Run Aviones.

Verify that the parameters had been updated by clicking on “**View**” followed by “**Physics Parameters**” as shown in Figure 41. The values of the parameters can also be changed from this user interface.

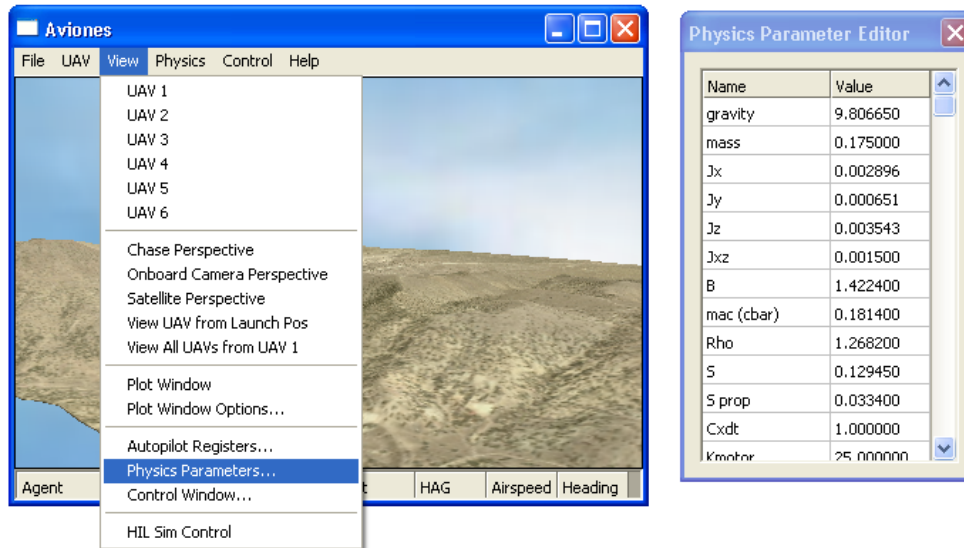


Figure 41. Physics parameter editor window

APPENDIX M. PID GAINS FOR PROTOTYPE ON KESTREL AUTOPILOT

The PID gains can be changed from the user interface of Virtual Cockpit. Click on “Settings” followed by “PID Values”.

The PID gains for the prototype on Kestrel autopilot are shown in Figure 42. Only the parameters shaded in yellow was changed. The remaining parameters were the default values used for Zagi UAV test platforms.

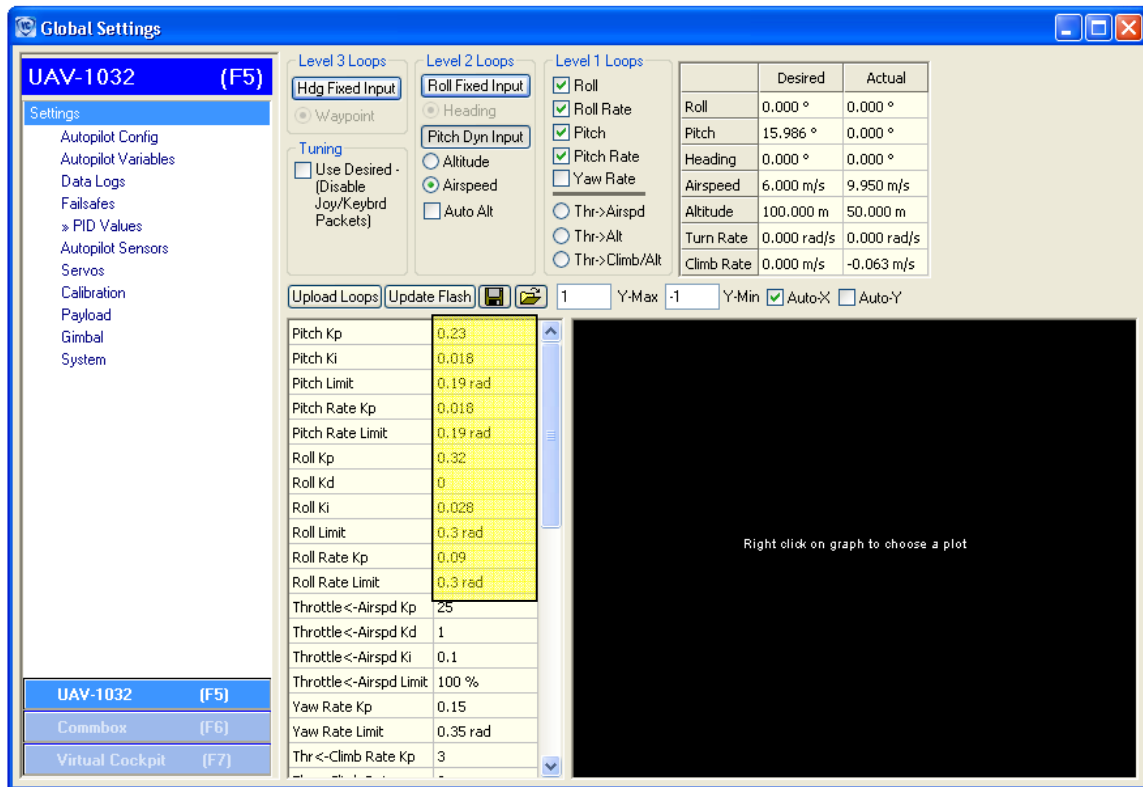


Figure 42. Values of PID gains

THIS PAGE INTENTIONALLY LEFT BLANK

APPENDIX N. PROCEDURES FOR RUNNING THE HIL EXPERIMENTS

As mentioned in Chapter VI, this was the first attempt to run HIL for Kestrel Autopilot. Therefore, this set of procedures is described in detail for the benefit of future works.

Set up the TCP/IP connection as described in Appendix J.

Create a test route for the respective velocity (6 m/s to 16 m/s at 2 m/s intervals), with waypoints 3 and 4 having a height difference of 300 m. Upload the test route to the autopilot using the flight plan control window (click on the red “Upld” tab) of Virtual Cockpit as shown in Figure 43.



Figure 43. Flight control window of Virtual Cockpit

Launch the UAV using the “UAV” tab in Aviones by clicking on “**Launch if necessary**” or “**Relaunch current UAV**” as shown in Figure 44.

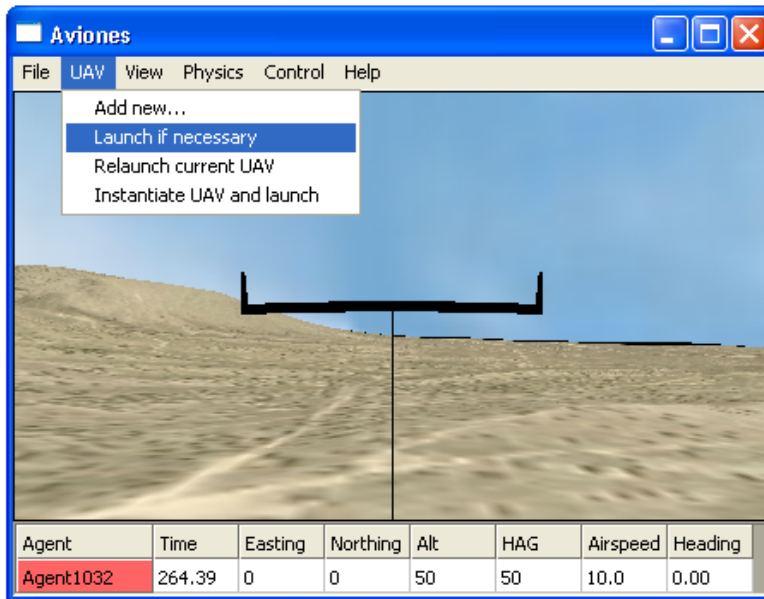


Figure 44. Launching the UAV from Aviones

Ensure that the UAV is in “Nav” mode and the autopilot is navigating to waypoint 1 as shown in Figure 45.

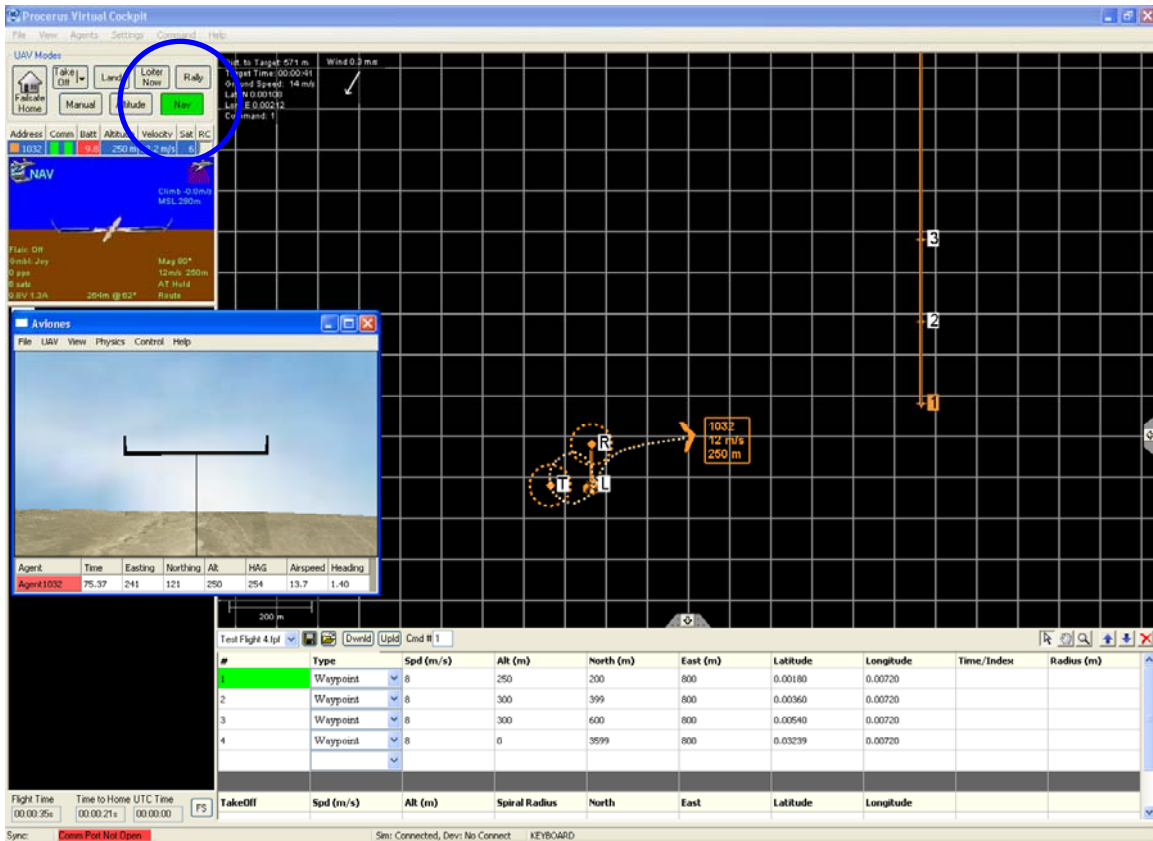


Figure 45. UAV in “NAV” mode

The benefit of using Virtual Cockpit’s default settings for the Zagi UAV test platform is that the Zagi is a powered glider. It is capable of autonomous flight toward the active waypoint with its onboard propeller motor.

When it has reach waypoint 3, which simulates the release point of the KUAV, it is necessary to “turn off” the propeller motor as the KUAV is a non-powered glider. This can be implemented through Aviones. Under the “**View**” menu in Aviones, open “HIL Sim Control” and click on the “**Engine Failure**” tab as shown in Figure 46. This will “turn off” the motor, but the autopilot is still navigating waypoints.

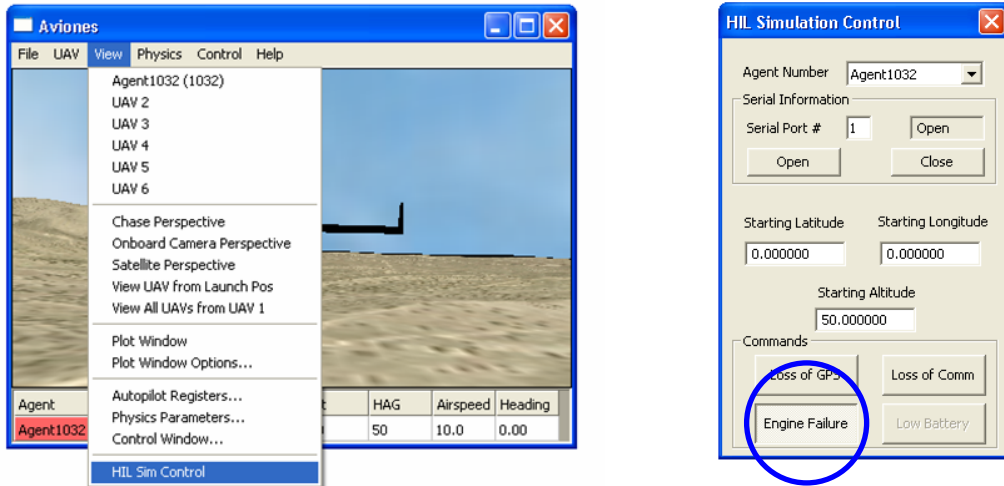


Figure 46. HIL Sim Control Window of Aviones

Virtual Cockpit has a data logging capability and this is extremely useful in recording the results for subsequent analysis. The data log can be activated by clicking “Settings” followed by “Data Logs”. The user interface is shown in Figure 47.

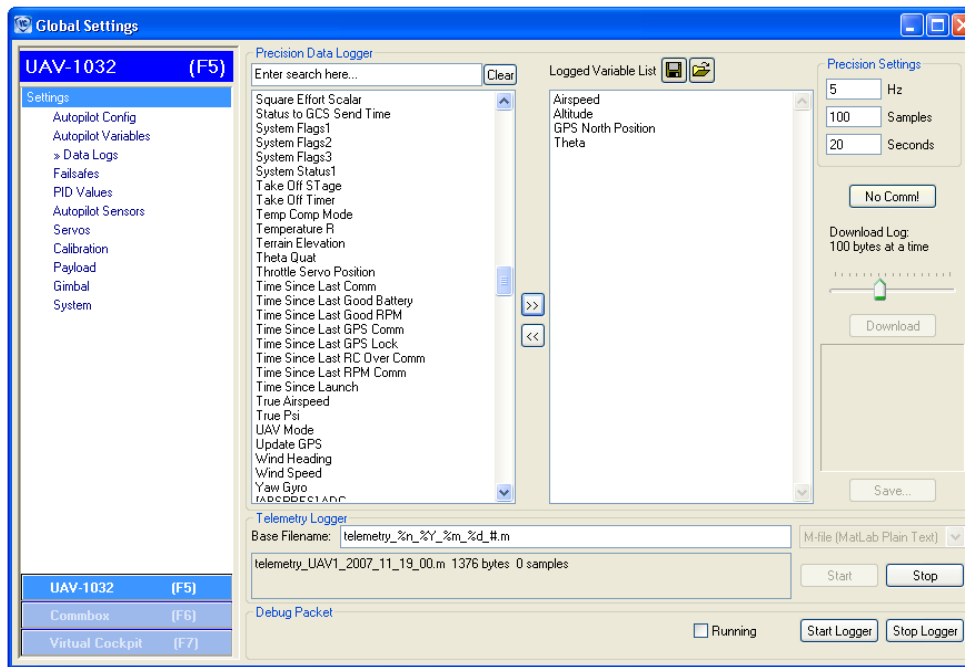


Figure 47. Data log window of Virtual Cockpit

Data logging commences moments before engine failure is activated to simulation the releasing of the KUAV from the HUAV.

Four data are recorded for analysis.

Airspeed, the speed at which the KUAV is descending after being released from the HUAV.

Altitude, the height of the KUAV during its descend after being released from the HUAV.

GPS North Position, the horizontal range which the KUAV had traveled during its descend after being released from the HUAV.

Theta, the pitch angle of the KUAV during its descend after being released from the HUAV.

When then altitude of the UAV reaches zero, this indicate that the UAV have landed.

The data for each run are saved as M-scripts and analyzed using Matlab. The following script is written to analyze the results and plot the respective graphs.

```
%Data analysis for HIL

clc;

test8ms;

data=datalog.samples;

E=data(:,1)./5;
P=data(:,3).*180/pi;
R=data(:,4);
V=data(:,5);
H=data(:,6);

glide=(data(100,6)-data(250,6))/(data(100,4)-data(250,4))
glide_deg=glide*180/pi

pitch=mean(data(100:250,3))
pitch_deg=pitch*180/pi

aoa_deg=pitch_deg-glide_deg

Velocity=mean(data(100:250,5))
```



```

Start_Time=data(1,1);
End_Time=data(316,1);
Endurance=(End_Time-Start_Time)/5

Start_R=data(1,4);
End_R=data(316,4);
Range=(End_R-Start_R)

figure (1);
hold on;

subplot(3,1,1)
plot(R,H);
axis equal;
xlabel('R - Horizontal Range (m)','fontsize',14);
ylabel('H - Altitude (m)','fontsize',14);
title('H vs. R','fontsize',16);
grid on;

subplot(3,1,2)
plot(E,P);
xlabel('E - Endurance (sec) ','fontsize',14);
ylabel('P - Pitch Angle (deg)','fontsize',14);
title('P vs. E','fontsize',16);
grid on;

subplot(3,1,3)
plot(E,V);
xlabel('E - Endurance (sec)','fontsize',14);
ylabel('V - Velocity (m/s)','fontsize',14);
title('V vs. E','fontsize',16);
grid on;
print -tiff -depsc 8ms.eps;

hold off;

```

Repeat the above procedures for the other test velocities.

APPENDIX O. SIMULATION RESULTS FROM HIL

Pitch	Glide Angle	AOA	R	E	Velocity	H	L/D
(deg)	(deg)	(deg)	(m)	(s)	(m/s)	(m)	
-5.06	-9.75	4.69	1752	288	6.0	300	5.84
-8.47	-10.99	2.52	1594	200	8.0	300	5.31
-10.79	-12.29	1.5	1449	144	10.0	300	4.83
-12.91	-13.53	0.62	1273	106	12.0	300	4.24
-15.07	-15.42	0.35	1122	81	14.0	300	3.74
-17.39	-17.51	0.12	977	63	16.2	300	3.26

THIS PAGE INTENTIONALLY LEFT BLANK

LIST OF REFERENCES

- [1] J. C. Wang, & Y. S. Chua, (2005). Unmanned Aerial Vehicle: Development Trends & Technology Forecast. *DSTA Horizons, 1*. Retrieved July 10, 2007, from <http://www.dst.gov.sg/index.php/DSTA-2005-Chapter-2/>.
- [2] J. T. Correll, (2002). From Sensor to Shooter. *Airforce Magazine Online*, 85. Retrieved July 10, 2007, from <http://www.afa.org/magazine/Feb2002/0202edit.asp>.
- [3] V. Dobrokhodov, I. Kaminer, K. D. Jones, & R. Ghabcheloo, (2006). Vision Based Tracking and Motion Estimation For Moving Targets Using Small UAVs. *American Institute of Aeronautics and Astronautics*. Retrieved July 10, 2007, from http://pdf.aiaa.org/preview/CDReadyMGNC06_1305/PV2006_6606.pdf.
- [4] General Atomics Aeronautical Systems. *Predator B* (2007). [Online Brochure] Retrieved July 10, 2007, from http://www.gas.com/products/pdf/Predator_B.pdf.
- [5] Sagem Défense Sécurité, *Sperwer* (2006). [Online Brochure] Retrieved July 10, 2007, from <http://www.sagem-ds.com/pdf/en/D719.pdf>.
- [6] AAI Corporation, *Shadow 200* (2006). [Online Brochure] Retrieved July 10, 2007, from http://www.aaicorp.com/New/UAS/Shadow200_08-23-07a.pdf.
- [7] Thales UK, *Watchkeeper Tactical UAV System* (2006). [Online Brochure] Retrieved July 10, 2007, from <http://www.army-technology.com/projects/watchkeeper/>.
- [8] Northeast Sailplanes Products, *Swift 2 Wing* (2007). [Online Brochure] Retrieved Oct 15, 2007, from <http://www.nesail.com/detail.php?productID=5482>.
- [9] Procerus Technologies, *KESTREL™ Autopilot 2.2* (2007). [Online Brochure] Retrieved July 10, 2007, from <http://www.procerusuav.com/productsKestrelAutopilot.php>.
- [10] J. Yost, *The EH Airfoils*. Retrieved July 10, 2007, from <http://www.b2streamlines.com/EH.html>.
- [11] *LinAir Version 3.4 User Manual*. (2003) Stanford, CA: Desktop Aeronautics, Inc.

- [12] G. E. Torres, & T. J. Mueller, (2001). Aerodynamic Characteristics of Low Aspect Ratio Wings at Low Reynolds Number. In T. J. Mueller (Ed.) *Fixed and Flapping Wing Aerodynamics for Micro Air Vehicle Application* (pp. 115-141). Virginia: American Institute of Aeronautics and Astronautics.
- [13] M. I. Lizarraga, (2004). Autonomous Landing System for a UAV (Master's Thesis, Naval Postgraduate School, Monterey, CA, 2004).
- [14] B. W. McCormick, (1995). *Aerodynamics Aeronautics and Flight Mechanics*. New York: John Wiley & Sons, Inc.
- [15] *Kestrel User Guide Version 1.7*. (2007). Vineyard, UT: Procerus Technologies.
- [16] *Kestrel Installation and Configuration Guide Version 1.7*. (2007). Vineyard: UT, Procerus Technologies.
- [17] *Piccolo Steps to Autonomous Flight Version 1.1*. (2003). Hood River: OR, Cloud Cap Technology.

INITIAL DISTRIBUTION LIST

1. Defense Technical Information Center
Ft. Belvoir, Virginia
2. Dudley Knox Library
Naval Postgraduate School
Monterey, California
3. Professor Anthony J. Healey
Chairman, Department of Mechanical and Astronautical Engineering (MAE)
Naval Postgraduate School
Monterey, California
4. Professor Vladimir N. Dobrokhodov
Naval Postgraduate School
Monterey, California
5. Professor Kevin D. Jones
Naval Postgraduate School
Monterey, California
6. Professor Yeo Tat Soon
Director, Temasek Defence System Institute (TDSI)
National University of Singapore
Singapore